PNAS RESEARCH ARTICLE | DEVELOPMENTAL BIOLOGY

Hypomorphic and dominant-negative impact of truncated SOX9 dysregulates Hedgehog–Wnt signaling, causing campomelia

Tiffany Y. K. Au[a,1], Raymond K. H. Yip[a,1,2], Sarah L. Wynn[a], Tiong Y. Tan[a,3], Alex Fu[b,4], Yu Hong Geng[a,5], Irene Y. Y. Szeto[a], Ben Niu[a,6], Kevin Y. Yip[b,7], Martin C. H. Cheung[a], Robin Lovell-Badge[c], and Kathryn S. E. Cheah[a,8]

Edited by Clifford Tabin, Harvard Medical School, Boston, MA; received June 10, 2022; accepted November 2, 2022

Haploinsufficiency for SOX9, the master chondrogenesis transcription factor, can underlie campomelic dysplasia (CD), an autosomal dominant skeletal malformation syndrome, because heterozygous *Sox9* null mice recapitulate the bent limb (campomelia) and some other phenotypes associated with CD. However, in vitro cell assays suggest haploinsufficiency may not apply for certain mutations, notably those that truncate the protein, but in these cases in vivo evidence is lacking and underlying mechanisms are unknown. Here, using conditional mouse mutants, we compared the impact of a heterozygous *Sox9* null mutation (*Sox9*$^{+/-}$) with the *Sox9*$^{+/Y440X}$ CD mutation that truncates the C-terminal transactivation domain but spares the DNA-binding domain. While some *Sox9*$^{+/Y440X}$ mice survived, all *Sox9*$^{+/-}$ mice died perinatally. However, the skeletal defects were more severe and IHH signaling in developing limb cartilage was significantly enhanced in *Sox9*$^{+/Y440X}$ compared with *Sox9*$^{+/-}$. Activating *Sox9*^{Y440X} specifically in the chondrocyte–osteoblast lineage caused milder campomelia, and revealed cell- and noncell autonomous mechanisms acting on chondrocyte differentiation and osteogenesis in the perichondrium. Transcriptome analyses of developing *Sox9*$^{+/Y440X}$ limbs revealed dysregulated expression of genes for the extracellular matrix, as well as changes consistent with aberrant WNT and HH signaling. SOX9^{Y440X} failed to interact with β-catenin and was unable to suppress transactivation of *Ihh* in cell-based assays. We propose enhanced HH signaling in the adjacent perichondrium induces asymmetrically localized excessive perichondrial osteogenesis resulting in campomelia. Our study implicates combined haploinsufficiency/hypomorphic and dominant-negative actions of SOX9^{Y440X}, cell-autonomous and noncell autonomous mechanisms, and dysregulated WNT and HH signaling, as the cause of human campomelia.

SOX9 | campomelic dysplasia | osteoblast differentiation | skeletal disorders | WNT and HH signaling

Significance

SOX9 heterozygous mutations cause skeletal malformation and bent bones of Campomelia Dysplasia. The cause of bent bones and whether similar molecular mechanisms apply in vivo for all heterozygous mutations in *SOX9* are unclear. In this study, we generated a mouse equivalent of the human CD *SOX9*^{Y440X} mutation, which truncates the C-terminal transactivation domain. We discovered, unlike the null mutation, heterozygosity for *Sox9*^{Y440X} exerts cell autonomous and noncell autonomous dominant-negative effects on WNT and HH signaling, dysregulating osteogenesis, causing campomelia. Our study provides mechanistic insight into *SOX9's* molecular control of human skeletal morphogenesis, that is relevant for normal control of bone shapes, life-limiting congenital growth defects, and the recapitulated processes of chondroosteogenesis in clinical scenarios such as during fracture repair.

During endochondral bone formation, chondrocytes in the cartilaginous growth plate differentiate in a highly regulated cascade of proliferation, cell-cycle exit and maturation, followed by phases of hypertrophy, culminating in transformation to become osteoblasts in the primary spongiosa (trabecular bone) (1–4). This differentiation cascade is regulated by transcription factors and signaling pathways, whose disruption results in skeletal dysplasias (5, 6). The SRY-box containing gene 9 (SOX9) transcription factor is a master regulator of chondrogenesis (7, 8). *SOX9* is first transcribed in bipotent osteochondroprogenitors and remains highly expressed in differentiating chondrocytes until they enter hypertrophy, but it is switched off in the osteogenic lineage (7, 9–14). Although SOX9 is crucial for the onset of chondrogenesis (8), it is not a pioneer transcription factor for establishing the chondrogenic program (15). SOX9 drives chondrocyte differentiation from bipotential osteochondroprogenitors through synergistic, antagonistic, and repressive actions in concert with partner factors to control the dynamic gene expression characteristic of the differentiation phases (reviewed in ref. 16). SOX9 directly activates many cartilage extracellular matrix (ECM) genes, including *Col2a1*, *Acan (Aggrecan), Col10a1*, *Col11a2*, as well as regulators of chondrocyte differentiation, such as *Sox5* and *Sox6,* many of which are severely down-regulated in developing mouse limb buds upon complete loss of SOX9 function (14, 15, 17–21). This robust transactivity is mediated by partner factors, such as SOX5 and SOX6 (themselves targets of SOX9) and AP1 (JUN), which act cooperatively with SOX9 (21–23). SOX9 is also required for the proliferation and survival of chondrocytes and prevents their osteoblastic conversion by antagonizing β-catenin and RUNX2 activity (14, 24–26).

SOX9 acts as a transactivator or a repressor during chondrocyte differentiation, depending on the context of cooperating factors, as illustrated by its regulation of *Col10a1* (27). In proliferating chondrocytes SOX9 binds directly to regulatory elements upstream of *Col10a1,* repressing its expression in concert with GLI factors, contributing to the specific restricted expression of *Col10a1* in hypertrophic chondrocytes (HCs) (20, 27). As chondrocytes enter hypertrophy, SOX9 binds to RUNX2, promoting its degradation and thus inhibiting RUNX2 transactivation of *Col10a1* (28). However, SOX9 also binds to the *Col10a1* promoter and, together with MEF2C, transactivates its expression in HCs (13). SOX9 and JUN cobined and coactivate a *Col10a1* enhancer, promoting hypertrophy (20, 23, 25, 27, 29). These interactions between factors and their binding to different cis-regulatory elements suggest a model of coordinated partnerships that drive the regulatory cascade of differential gene

Author contributions: T.Y.K.A., R.K.H.Y., S.L.W., and K.S.E.C. designed research; T.Y.K.A., R.K.H.Y., S.L.W., T.Y.T., A.F., Y.H.G., I.Y.Y.S., and M.C.H.C. performed research; M.C.H.C. contributed new reagents/analytic tools; T.Y.K.A., R.K.H.Y., T.Y.T., A.F., Y.H.G., B.N., K.Y.Y., R.L.-B., and K.S.E.C. analyzed data; T.Y.K.T., K.Y.Y., M.C.H.C., and R.L.-B. edited the paper; K.S.E.C. procured research funding; K.S.E.C. supervised research; and T.Y.K.A., R.K.H.Y., A.F., and K.S.E.C. wrote the paper.

The authors declare no competing interest.

This article is a PNAS Direct Submission.

This article contains supporting information online at https://www.pnas.org/lookup/suppl/doi:10.1073/pnas.2208623119/-/DCSupplemental.

Published December 30, 2022.

expression and signaling pathways controlling chondrocyte differentiation during endochondral bone formation, disruption of which results in skeletal dysplasia in humans and mice (14, 21, 23, 26, 29).

Heterozygosity for point mutations (missense, nonsense, frameshift, and splice site) in *SOX9,* as well as chromosomal aberrations outside the *SOX9* gene that presumably disturb key regulatory regions, cause campomelic dysplasia (CD; OMIM 114290) (30–35), a rare, dominant semi-lethal skeletal disease characterized by congenital shortening and angulation of long bones (campomelia). Other frequent anomalies include hypoplastic scapulae, Pierre Robin sequence, sensorineural deafness, and sex reversal or urogenital anomalies in affected karyotypic males (36, 37). The molecular, cellular, and developmental abnormalities leading to campomelia in CD patients are not well defined. Because mutations in a single allele of *SOX9* are sufficient to cause CD without obvious genotype–phenotype correlations (38) and heterozygous null $Sox9^{+/-}$ mice phenocopy the skeletal dysmorphology of CD (39), it is generally believed that CD is caused by haploinsufficiency for *SOX9*. However, the haploinsufficiency model assumes all mutations lead to loss-of-function and does not consider the diverse mutational spectrum in SOX9 and CD (14, 32, 35, 38, 40).

The $SOX9^{Y440X}$CD mutation, which introduces a premature termination codon, truncating the C-terminal transactivation domain (residues 402 to 509), is the most commonly reported mutation, possibly because heterozygous $SOX9^{Y440X}$individuals survive longer than other individuals with CD (38, 41–43). $SOX9^{Y440X}$ has been shown to retain DNA binding and residual transactivation activity in vitro (42, 43), suggesting $SOX9^{Y440X}$may be a hypomorphic allele. A recent cell-based study of four other *SOX9* CD-associated nonsense mutations that truncate the C terminus has raised the possibility of a dominant-negative effect and mechanisms other than haploinsufficiency for null mutations (44). Whether any of these mechanisms act in combination has not been addressed in vivo.

In this study, we compare the in vivo pathophysiological consequences on skeletal development of heterozygosity for the truncating $SOX9^{Y440X}$ CD mutation with a *SOX9* null mutation in mice genetically altered to carry equivalent mutations. Combined with transcriptomic analyses and in vitro and in vivo transactivation assays, we present evidence that, rather than a single haploinsufficiency mechanism, $SOX9^{Y440X}$ exerts a combination of haploinsufficiency/hypomorphism and dominant-negative mechanisms on WNT–HH signaling that, together with noncell autonomous effects, perturbs perichondrial osteogenesis, resulting in campomelia.

CD-Like Phenotypes Were More Severe in $Sox9^{+/Y440X}$ Mutants than for $Sox9^{+/-}$ Mice

To overcome the perinatal lethality associated with heterozygosity for *Sox9* (39), and to elucidate the pathological mechanisms of the $SOX9^{Y440X}$ CD mutation, we generated a mouse model harboring a conditional *Sox9* allele, $Sox9^{floxed\text{-}Y440X}$. This permits transcription of WT *Sox9* in the absence of Cre protein, but following Cre recombination, $Sox9^{Y440X}$ and a linked *EGFP* reporter are transcribed in its place (Fig. 1*A* and *SI Appendix*, Fig. S1), with the same temporal and tissue specificity in vivo. Mice homozygous for the $Sox9^{floxed\text{-}Y440X}$ allele were healthy and fertile. To compare the in vivo impact of a null with the Y440X mutation, we generated $Sox9^{+/-}$ and $Sox9^{+/Y440X}$ constitutive heterozygous mutant mice (with the latter named $Sox9^{+/CD}$ hereafter) by crossing conditional $Sox9^{floxed}$ (7) and $Sox9^{floxed\text{-}Y440X}$ mice to *β-actin-Cre* (ubiquitous Cre activity) mice (31). EGFP activity in $Sox9^{+/CD}$ embryos mirrored the typical *Sox9* expression pattern observed in $Sox9^{+/IRES\text{-}EGFP}$mice (12), confirming that the $Sox9^{Y440X}$-IRES-EGFP cassette was controlled by the endogenous *Sox9* promoter (Fig. 1*B*).

Skeletal preparations of $Sox9^{+/-}$ and $Sox9^{+/CD}$ neonates showed skeletal and craniofacial abnormalities that recapitulated those of human CD patients, including campomelia, hypoplastic scapula, malformed spine, small thoracic cage, hypoplastic tracheal cartilage, cleft palate, and micrognathia (Fig. 1 *C–E* and *SI Appendix*, Tables S1 and S2). $Sox9^{+/CD}$mice displayed shorter mandibles, ribs, and appendicular bones, and the campomelia and spine defects were more severe than for $Sox9^{+/-}$ mice (*SI Appendix,* Tables S1 and S2). By contrast, cleft palate and tracheal cartilage defects were milder in $Sox9^{+/CD}$than in $Sox9^{+/-}$ mice (Fig. 1 *D* and *E* and *SI Appendix,* Table S2). Consistent with a previous report, all $Sox9^{+/-}$ mice died shortly after birth of respiratory distress (39), whereas 10% of $Sox9^{+/CD}$ mice survived to adulthood (*SI Appendix*, Tables S1 and S2). The surviving $Sox9^{+/CD}$ mice had kinked tails and kyphosis and were stunted compared with $Sox9^{+/+}$ mice (WT) mice (Fig. 1 *F* and *G*). Like some CD patients (37), they also displayed sensorineural deafness (*SI Appendix*, Tables S1 and S2). Therefore, we hypothesize that $Sox9^{Y440X}$ is not simply a loss of function mutation, but other mechanisms could apply.

Enhanced Osteogenesis in Embryonic Limbs of $Sox9^{+/CD}$ Mice

To investigate the pathology of campomelia, we compared the fetal skeletons of $Sox9^{+/CD}$ and $Sox9^{+/-}$ mice using morphometric and molecular assays. Alcian Blue staining revealed severely bent tibia in E15.5 $Sox9^{+/CD}$ fetuses, deviation of the orientation of the growth plate to the main axis and an expanded domain of hypertrophic cartilage and tissue mass located asymmetrically adjacent to the perichondrium (hereafter referred to as "perichondrial mass"), which was not present in WT and $Sox9^{+/-}$ mice (Fig. 2*A*). Microcomputed tomography (μCT) imaging confirmed the osseous nature of the perichondrial mass and a more severe campomelia in $Sox9^{+/CD}$ mice compared with $Sox9^{+/-}$ (Fig. 2*B*).

Collagen X (*Col10a1)* is synthesized exclusively by prehypertrophic chondrocytes (PHCs) and HCs from E13.5 onward. *Col10a1* is not expressed in the perichondrium and is down-regulated in HCs in the lower hypertrophic zone (late HCs) as they transform to become osteoblasts (3). Osterix (OSX) is expressed by PHCs, HCs, and osteoblasts (Fig. 2 *C* and *D*) (3, 45). The cells in the perichondrial mass in $Sox9^{+/CD}$ tibia were strongly positive for OSX and *Col1a1* transcripts, confirming the osteogenic nature of the tissue (Fig. 2 *C–E*). Notably, chondrocytes in the proliferative zone of $Sox9^{+/-}$ mice expressed *Col1a1* transcripts, which is consistent with a previous report that SOX9 prevents osteoblastic conversion of chondrocytes (13). Few cells in the lower part of the hypertrophic zone of $Sox9^{+/CD}$ tibia expressed *Col10a1* transcripts even though the surrounding ECM in the whole region stained strongly for collagen X protein (compare Fig. 2 *C* and *E*). In addition, *Col1a1* was expressed in the lower part of the hypertrophic zone (Fig. 2*E*). This discordant expression pattern suggests that $Sox9^{+/CD}$ HCs ceased *Col10a1* transcription prematurely and had initiated osteogenesis. In agreement, expression of *Mmp13* and *Opn* (both late HC (LHC) markers) was strongly up-regulated (Fig. 2 *F* and *G*).

Notably, $Sox9^{+/CD}$ mice showed a marked increase of *Ihh* expression in PHCs and of its downstream transcriptional target, *Ptch1*, in the proliferating chondrocytes (PCs) and perichondrium (Fig. 2*H*). By contrast upregulation of these two markers was milder in $Sox9^{+/-}$in comparison with $Sox9^{+/+}$, paralleling the differing skeletal severity in these strains (Fig. 2*H*). In E13.5 tibiae, before the formation of the primary ossification center and overt campomelia, *Ptch1* RNA signals were stronger in the $Sox9^{+/CD}$ growth plate compared with $Sox9^{+/-}$ and $Sox9^{+/+}$. Probing for *Ihh* and *Col10a1* transcripts confirmed normal chondrocyte differentiation to the hypertrophic state in E13.5 $Sox9^{+/-}$and $Sox9^{+/CD}$ mice. Importantly, more *Col1a1*-expressing cells was already apparent in the perichondrium of E13.5 $Sox9^{+/-}$ and $Sox9^{+/CD}$ tibia than that of $Sox9^{+/+}$, consistent with accelerated onset of osteogenesis (*SI Appendix,* Fig. S2*A*). Taken together, the data suggest premature HC differentiation and aberrant perichondrial osteogenesis may contribute to the development of campomelia.

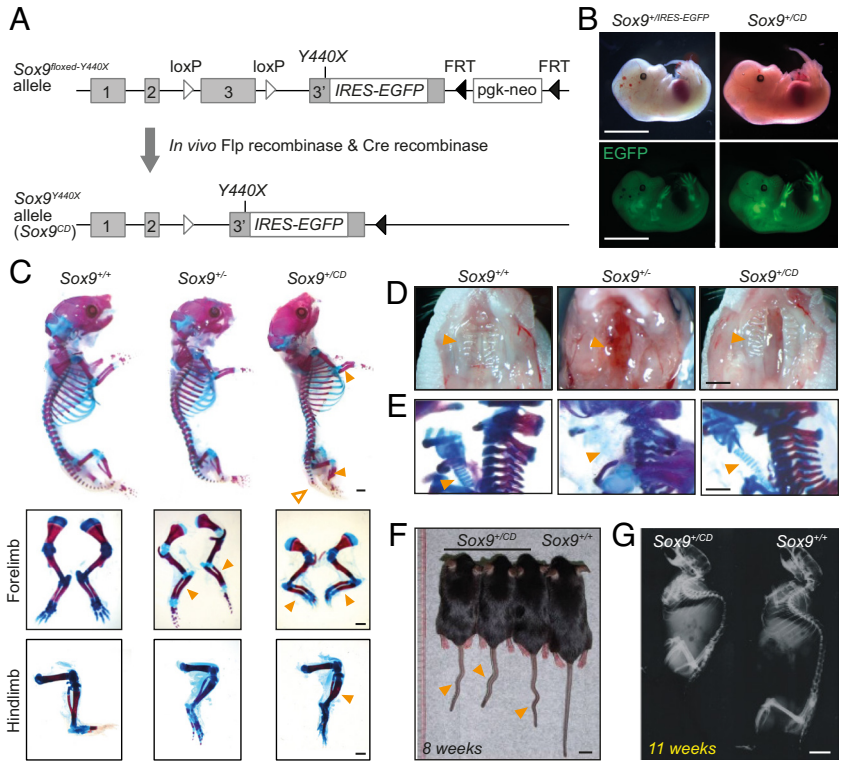

Fig. 1. *Sox9*$^{+/CD}$mice recapitulate human CD phenotypes. (*A*) Schematic representation of the *Sox9*^{Y440X} allele that expresses *Sox9*^{Y440X} and the *IRES-EGFP* cassette in the presence of Cre recombinase. (*B*) Brightfield and fluorescence images of E15.5 *Sox9*$^{+/IRES-EGFP}$ and *Sox9*$^{+/Y440X\text{-}IRES\text{-}EGFP}$ (*Sox9*$^{+/CD}$) embryos ($n = 3$). (*C*) Alcian blue and Alizarin red staining of skeletal preparations of *Sox9*$^{+/+}$*Sox9*$^{+/-}$, and *Sox9*$^{+/CD}$ newborns ($n = 3$). Magnified views of the forelimb and the hindlimb are provided. Filled arrowheads point to campomelia in appendicular bones and open arrowhead points to the kinked tail in *Sox9*$^{+/CD}$ mice. (*D* and *E*) Brightfield (*D*) and skeletal preparation (*E*) images of the trachea in *Sox9*$^{+/+}$*Sox9*$^{+/-}$, and *Sox9*$^{+/CD}$ newborns ($n = 5$). Arrowheads point to the tracheal cartilage. (*F* and *G*) Brightfield (*F*) and radiography (*G*) of 8-wk (*F*) and 11-wk-old (*G*) *Sox9*$^{+/+}$ and *Sox9*$^{+/CD}$ mice ($n = 3$). Arrowheads indicate the kinked tail in *Sox9*$^{+/CD}$ mice. (Scale bar, 1 cm (*B*, *F*, and *G*), 1 mm (*C*, *D*, and *E*).)

Sox9^{Y440X} Affects Both Perichondrial and HC Lineages, Inducing Campomelia

Two sources of osteoblasts contribute to the development of appendicular skeleton: osteoprogenitors in the perichondrium and HCs (3, 4, 46). Since SOX9 inhibits osteogenesis (13, 26), we tested whether the accelerated HC maturation in *Sox9*$^{+/CD}$ altered the progression of HC-osteoblast differentiation and contributed to campomelia. We utilized the HC-specific *Col10a1*^{Cre} knock-in line (abbreviated as *C10*) (3) to activate the *Sox9*^{Y440X} mutation in pre-HCs and HCs but not in the perichondrium (3), and traced their fate with a Cre-dependent *R26R*^{tdTomato} reporter strain (*TdT*) (47) (Fig. 3*A*). *Sox9* transcripts are expressed strongly in PCs and PHCs, at very low levels in the perichondrium and are absent in HCs (11, 48), although protein persists in less mature HCs in the upper part of the hypertrophic zone (Fig. 3*B*) (13). To detect SOX9^{Y440X} protein, we generated an antibody that specifically recognizes the mutant protein but not WT SOX9 (see *Methods*). In both *C10Sox9*$^{+/CD}$;*TdT* and *C10Sox9*$^{CD/CD}$;*TdT* mice, only WT SOX9 protein was present in the resting and PCs, whereas SOX9^{Y440X} was present in pre-HCs and HCs (Fig. 3*B*). In these conditional heterozygous mutant mice, SOX9^{Y440X} was coexpressed with WT SOX9 in the less differentiated HCs in the upper part of the hypertrophic zone (Fig. 3*B*). Unlike WT SOX9, SOX9^{Y440X} was expressed throughout the hypertrophic zone in homozygous conditional mutants (Fig. 3*B*), suggesting SOX9^{Y440X} protein was not only stable but persisted longer.

C10Sox9$^{+/CD}$;*TdT* mice displayed comparable appendicular bone lengths to their control littermates but homozygous *C10Sox9*$^{CD/CD}$;*TdT* neonates displayed generalized shortening of endochondral long bones, and this phenotype persisted into adulthood, implicating a dose-dependent impact of SOX9^{Y440X} (Fig. 3*C* and *SI Appendix*, Fig. S3 *A* and *B*). Three-dimensional reconstruction of μCT images and morphometric analyses did not show differences in trabecular bone volume and quality between control and heterozygous conditional mutants but revealed significant anterolateral bowing in the tibiae of *C10Sox9*$^{CD/CD}$;*TdT* homozygotes (Fig. 3*D* and *SI Appendix*, Fig. S3 *C–F*). However, the severity of campomelia was milder in *C10Sox9*$^{CD/CD}$;*TdT* compared with *Sox9*$^{+/CD}$ mice, implying *Sox9*^{CD} activity in the non-*Col10*-marked cell population (i.e., non-HC derivatives) also contribute to the full campomelia (Figs. 1*C* and 3*C*). Interestingly, *C10Sox9*$^{CD/CD}$;*TdT* mice displayed stronger and broader activation of *Mmp13* and *Opn* (*Spp1*) in the hypertrophic cartilage and enhanced *Col1a1* signal in the perichondrium flanking the primary ossification center, implying an increase in LHCs and accelerated perichondrial osteogenesis (Fig. 3*E*). These data suggest that SOX9^{Y440X} activity in pre-HCs/HCs and the HC-osteoblast lineage combined with activity in the other chondrocyte populations (e.g., PCs) together causes the full campomelia phenotype in constitutive *Sox9*$^{+/CD}$ mice.

SOX9^{Y440X} Does Not Affect the Rate of HC-Osteoblast Differentiation

We next assessed whether SOX9^{Y440X} affects the survival of HCs and their rate of differentiation to osteoblasts. TUNEL assays showed no precocious cell death of *Sox9*^{Y440X}-expressing HCs (*SI Appendix*, Fig. S4*A*). To determine whether the increased osteogenesis was caused by enhanced transition of HCs to osteoblasts in trabecular bone, we quantified the relative proportions of three cell populations in trabecular bones of the conditional mutant neonates: HC-derived cells (tdTomato$^+$), HC-derived mature osteoblasts (*Col1a1*$^+$tdTomato$^+$), and non-HC derived mature

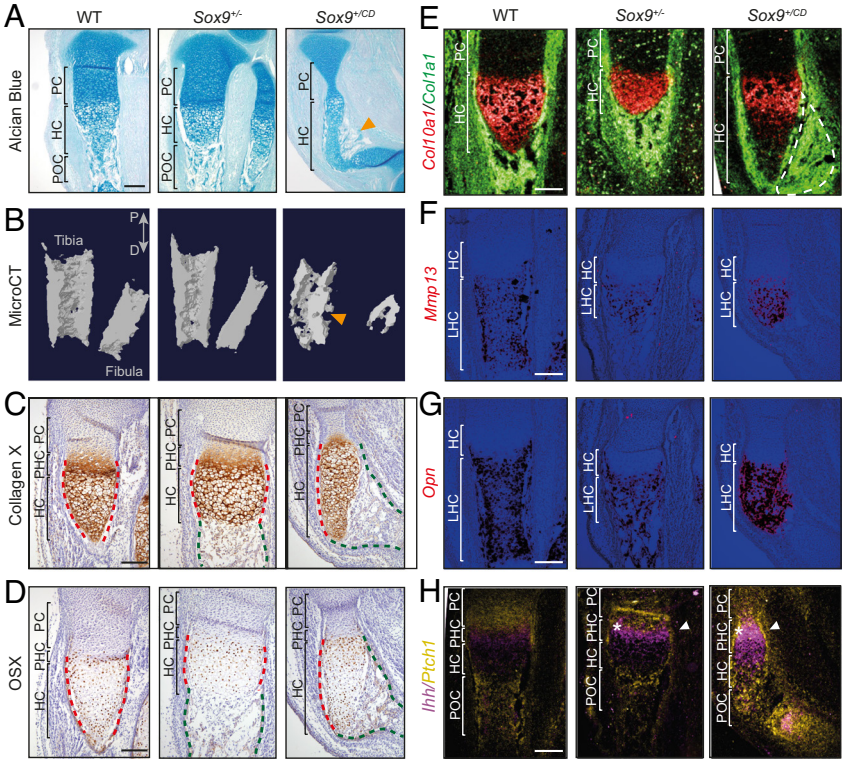

Fig. 2. Enhanced osteogenesis in bent limbs of $Sox9^{+/CD}$mice. (*A* and *B*) Alcian blue staining (*A*) and MicroCT (*B*) of E15.5 tibiae of $Sox9^{+/+}Sox9^{+/-}$, and $Sox9^{+/CD}$ mice. Arrowheads point to the ossified perichondrial tissue. $n = 3$ (*A*) and 5 (*B*). (*C* and *D*) Immunohistochemistry for Collagen X (*C*) and Osterix, OSX (*D*) in E15.5 tibiae of $Sox9^{+/+}Sox9^{+/-}$, and $Sox9^{+/CD}$ mice ($n = 3$). Red dotted lines mark the hypertrophic zone. Green dotted lines demarcate the primary ossification center. (*E–H*) In situ hybridization for *Col10a1* and *Col1a1* (*E*), *Mmp13* (*F*), *Opn* (*G*), and *Ihh* and *Ptch1* (*H*) in E15.5 tibiae of $Sox9^{+/+}Sox9^{+/-}$, and $Sox9^{+/CD}$ mice ($n = 3$). Dotted line circles the expanded perichondrial mass in $Sox9^{+/CD}$ mice. Arrowheads indicate enhanced *Ptch1* signal in the perichondrium. Asterisks denote enhanced *Ihh* signal in PHC. PC, proliferating chondrocytes; PHC, prehypertrophic chondrocytes; HC, hypertrophic chondrocytes; LHC, late hypertrophic chondrocytes; POC, primary ossification center. (Scale bar, 100 μm (*A* and *C–H*).)

osteoblasts ($Col1a1^{+}$tdTomato^{-}) (*SI Appendix*, Fig. S4*B*). In line with previous reports (3, 4, 29), approximately 46.5 ± 3.5% of trabecular osteoblasts in control mice were HC descendants, but this percentage did not differ significantly between genotypes, implying the relative contribution of HCs to osteoblasts was not affected by $SOX9^{Y440X}$ (*SI Appendix*, Fig. S4 *C* and *D*).

To test whether there was a change in the kinetics of HC-osteoblast differentiation, we utilized mice carrying a tamoxifen-inducible *Col10a1-CreERt* allele (referred as *iC10* hereafter) (3) to activate $Sox9^{Y440X}$ in HCs and tracked their fate with *TdT*. We induced Cre activity in HCs by administrating tamoxifen at day 16.5 of pregnancy and fetuses were harvested at 16-, 24-, and 32 h postinjection (hpi). HC-descendants were quantified across five subchondral zones immediately below the chondro–osseous junction (zones 1 to 5, each 50 μm apart) (*SI Appendix*, Fig. S4*E*). At 16 hpi, majority of HC descendants were found within 100 μm from the junction and only around 10% of them expressed *Col1a1*. At 24 hpi and 32 hpi, an increasing proportion of HC descendants had transited into zones 4 and 5, and approximately 20% of the tdTomato^{+} cells had differentiated into *Col1a1*-expressing osteoblasts (*SI Appendix*, Fig. S4 *F* and *G*). These findings are consistent with previous reports showing that HCs differentiate into osteoblasts within ~24 h (3). At all experimental time points, the proportion of HC-derived osteoblasts remained comparable between control and mutant littermates. Similarly, there were no significant differences in the distribution pattern of HC-derived osteoblasts in the primary ossification center across various genotypes and timepoints (*SI Appendix*, Fig. S4 *F* and *G*). Although SOX9 normally inhibits osteogenesis (13, 26), the constitutive and inducible HC lineage tracing data indicate that $SOX9^{Y440X}$ does not alter the rate of HC-osteoblast differentiation. These results are consistent with a recent study on mature mice, which indicated deletion of *Sox9* did not affect the osteogenic fate of growth plate chondrocytes (26).

Conditional Deletion of SOX9 in HCs Does Not Result in Campomelia

We next tested whether campomelia in $C10Sox9^{CD/CD}$;*TdT* mutants is caused by deficiency of WT SOX9. We compared HC-specific conditional *Sox9* null mice (abbreviated as $C10Sox9^{c/c}$;*TdT*) with $C10Sox9^{CD/CD}$;*TdT* mutants. In situ hybridization revealed premature cessation of *Sox9* transcription in the pre-HCs of $C10Sox9^{c/c}$;*TdT* mutants, confirming effective inactivation of *Sox9*. SOX9 protein persists longer than its transcript (13). In $C10Sox9^{c/c}$;*TdT* mutants, SOX9 protein was depleted in HCs in the lower hypertrophic zone (*SI Appendix*, Fig. S5*A*). In contrast to $C10Sox9^{CD/CD}$;*TdT* mutants, $C10Sox9^{c/c}$;*TdT* neonates were grossly normal and did not exhibit campomelia (Fig. 3*D* and *SI Appendix*, Fig. S5 *B* and *C*). Double staining for *Col1a1* RNA and tdTomato lineage marker demonstrated that SOX9 deficiency in HCs did not perturb their differentiation to osteoblasts (*SI Appendix*, Fig. S5 *D* and *E*). Expression of *Ihh* and *Ptch1* was also unaffected in $C10Sox9^{c/c}$;*TdT* mutants (*SI Appendix*, Fig. S5*F*). These data together suggest that campomelia in $C10Sox9^{CD/CD}$;*TdT* mutants is not simply due to the loss of SOX9 activity but likely a consequence of other effects, acting noncell autonomously and/or dominant negatively.

Enhanced Chondrocytic IHH Signaling and Noncell Autonomous Stimulation of Perichondrial Osteogenesis

Osteoblast progenitors in the perichondrium migrate with invading blood vessels to populate the primary ossification center and contribute to trabecular bone (46). We next assessed possible

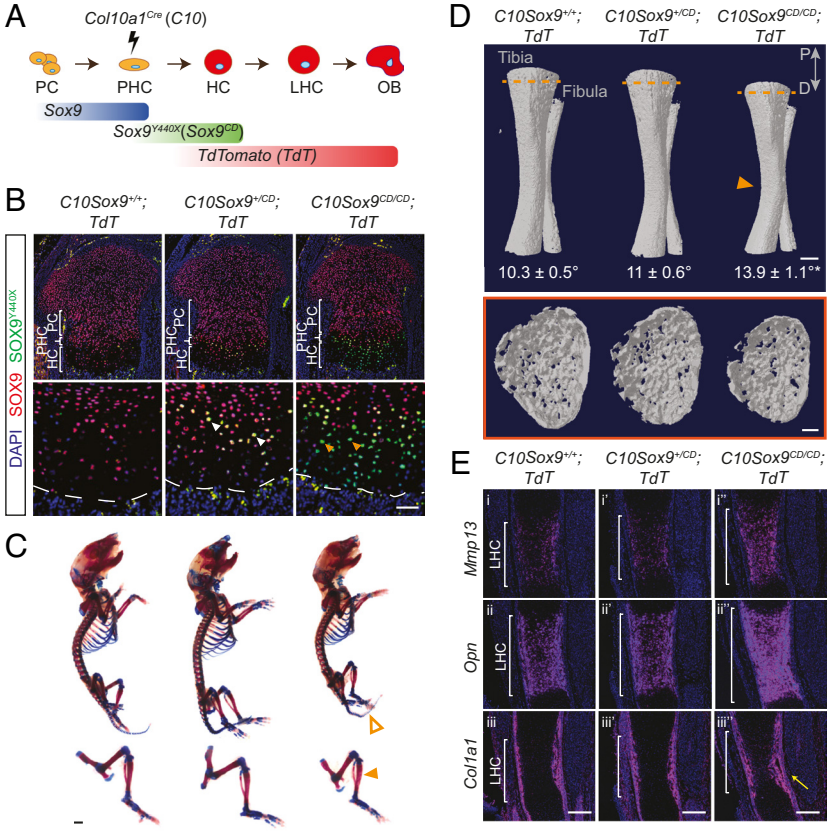

Fig. 3. Conditional activation of *Sox9*^{Y440X} in PHCs and HCs induces mild campomelia. (*A*) Schematic of the strategy to activate *Sox9*^{Y440X} (abbreviated as *Sox9*^{CD}) mutation in PHCs and HCs using *Col10a1*^{Cre} mouse line (abbreviated as *C10*) and trace their fate with a Cre-dependent TdTomato reporter allele, *R26R*^{TdTomato} (abbreviated as *TdT*). (*B*) Immunostaining for SOX9 and SOX9^{Y440X} in tibia of mice of the indicated genotype (n = 2). White arrowheads point to HCs that contain both SOX9 and SOX9^{Y440X}, and orange arrowheads point to HCs that contain SOX9^{Y440X} exclusively. Dotted lines demarcate the chondro–osseous junction. (*C*) Alcian blue and Alizarin red staining of skeletal preparations of newborn mice of the indicated genotype (n = 6). Open and filled arrowheads point to the kinked tail and campomelia, respectively. (*D*) MicroCT (*Top*) and 3D reconstruction of tibial trabecular bone (*Bottom*) of postnatal day 5 mice of the indicated genotype. Arrowhead points to campomelia. Measurements of bone bending (angle of deviation from the midline of the bone) are provided for each genotype. Significant bone bending was observed in *C10Sox9*$^{CD/CD}$*;TdT* when compared with *C10Sox9*$^{+/+}$*;TdT* (*P = 0.0002), but not with *C10Sox9*$^{+/CD}$*;TdT* mice (P = 0.0543) (n > 5). P: proximal, D: distal. (*E*) In situ hybridization for *Mmp13*, *Opn*, and *Col1a1* in E15.5 tibia of mice of the indicated genotype (n = 3). Brackets indicate late hypertrophic chondrocytes (LHC). Arrow points to enhanced ossification in perichondrium. PC, proliferating chondrocytes; PHC, prehypertrophic chondrocytes; HC, hypertrophic chondrocytes. (Scale bar, 50 μm (*B*), 1 mm (*C*), 0.5 mm (top row in *D*), 100 μm (bottom row in *D* and *E*).) *P* values were calculated using a one-way ANOVA followed by Tukey's multiple comparisons test. NS, not significant. All data reflect mean ± SEM.

stimulation of osteogenesis via noncell autonomous effects on the perichondrium using C10-mediated activation of SOX9^{Y440X} in HCs only (3).

Like E15.5 *Sox9*$^{+/CD}$ mice, E16.5 *C10Sox9*$^{CD/CD}$*;TdT* mice showed asymmetric and excessive ossification of their tibiae. This is in contrast to a symmetrically ossified cuff-like bone collar seen in *C10Sox9*$^{+/CD}$*;TdT,* and control littermates (Fig. 4 *A* and *B*). The extra perichondrial bone mass was not caused by increased cellular proliferation, as a 2-h EdU pulse showed no difference in the percentage of proliferating perichondrial cells between genotypes. Immunostaining for the tdTomato lineage marker confirmed the ossified mass was not derived from HC descendants, implying a perichondrial origin for the enhanced osteogenesis (Fig. 4*C*). We therefore hypothesized that SOX9^{Y440X} in pre-HCs/HCs stimulated perichondrial osteoblastogenesis via a noncell autonomous mechanism.

Ihh is expressed primarily in pre-HCs and signals to the perichondrium to induce bone collar formation (48–50). Similiar to *Sox9*$^{+/CD}$ mutant, in *C10Sox9*$^{CD/CD}$*;TdT* PHCs *Ihh* in situ hybridization signals were increased and the expression of *Ptch* and *Gli1*, both known transcriptional targets of the hedgehog pathway, was enhanced not only in proliferating and resting chondrocytes but also in the adjacent tibia perichondrium (Fig. 4*D*). A similar pattern of *Ihh* pathway upregulation was observed in the bones of E16.5 *C10Sox9*$^{CD/CD}$*;TdT* pups (*SI Appendix,* Fig. S6 *A* and *B*). EdU assays showed an increase in PCs and an increased numbers in perichondrial OSX^{+} osteoblast precursors in *C10Sox9*$^{CD/CD}$*;TdT* mutants, both of which are well-known readouts of chondrocytic IHH signaling to the perichondrium (Fig. 4 *E*–*H*). This effect is likely to be noncell autonomous, since *SOX9*^{Y440X} is not expressed in the perichondrium at this stage (Fig. 3*B*).

Regulation of ECM Genes and Wnt Signaling Are Perturbed in *Sox9*$^{+/CD}$ Developing Limbs

To gain insight into the molecular signaling pathways affected by SOX9^{Y440X} in vivo, we FACS purified *Sox9*-expressing (GFP^{+}) and non *Sox9*-expressing (GFP^{-}) cells from forelimb and hindlimb buds of E13.5 *Sox9*$^{+/IRES\text{-}EGFP}$(WT) (51) and *Sox9*$^{+/CD}$(CD) embryos for RNA-seq (Fig. 5*A* and *SI Appendix,* Fig. S7*A*). We assigned the forelimb and the hindlimb as biological replicates to increase statistical power (see *Methods* and *SI Appendix,* Fig. S7*B*). Consistent with the heterozygous nature of both mouse genotypes, the relative abundances of *Sox9*^{Y440X} and *Sox9* transcripts in GFP^{+} cells of *Sox9*$^{+/CD}$ embryos were equivalent (*SI Appendix,* Fig. S7*C*).

Comparing populations by multidimensional scaling revealed that GFP^{+} and GFP^{-} cells of *Sox9*$^{+/CD}$ limb buds show different gene expression profiles to their counterparts in *Sox9*$^{+/+}$ embryos (Fig. 5*B*). A total of 303 differentially expressed genes (DEGs) were identified, of which 227 genes were down-regulated and 76 were up-regulated (Fig. 5 *C* and *D*). Gene Ontology (GO) analysis of down-regulated genes revealed enrichment for genes involved in bone and cartilage

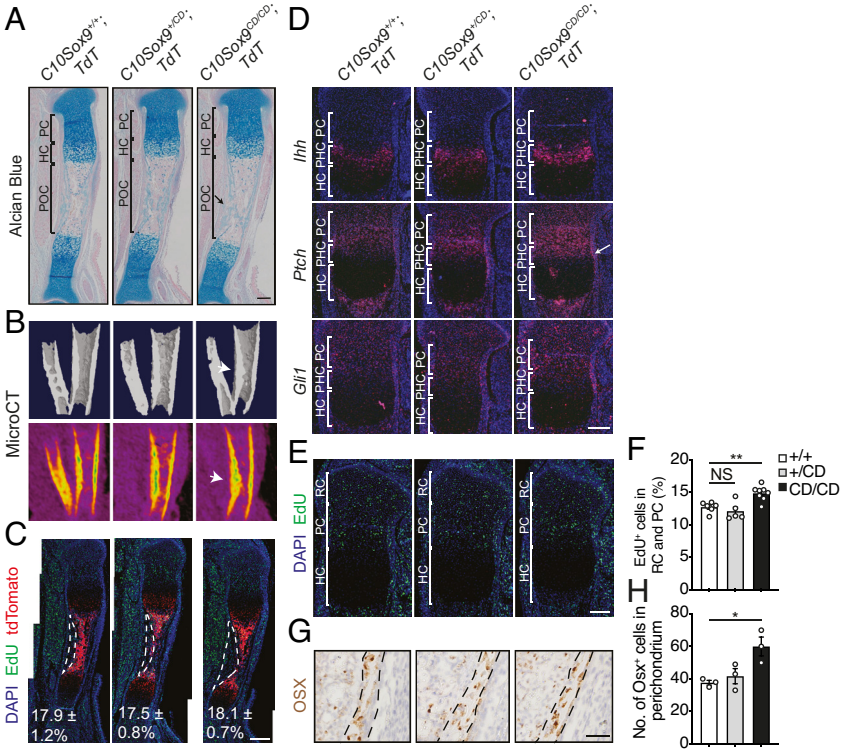

Fig. 4. Expression of *Sox9*^{Y440X} in PHCs/HCs promotes perichondrial hyperossification via the IHH pathway. (*A* and *B*) Alcian blue staining (*A*) and microCT (*B*) of E16.5 tibia of mice of indicated genotype ($n > 3$). Arrows point to enhanced perichondrial ossification. (*C*) Immunolabeling for TdTomato and 5-ethynyl-2′-deoxyuridine (EdU) click staining of E16.5 tibiae of mice of the indicated genotype ($n = 3$). Dashed lines circle the perichondrium. Percentages of EdU$^+$ perichondrial cells are provided with no significant difference detected across genotypes. (*D*) In situ hybridization for *Ihh*, *Ptch*, and *Gli1* in E16.5 tibia of mice of indicated genotype ($n = 3$). (*E* and *F*) EdU click staining (*E*) and quantification (*F*) of EdU$^+$ resting chondrocytes (RC) and proliferating chondrocytes (PC) of E16.5 tibia of mice of indicated genotype. Individual dots are from one bone. (*G* and *H*) Immunohistochemistry for Osterix (OSX) and quantification (*H*) of OSX$^+$ cells in the perichondrium of E16.5 tibia of mice of the indicated genotype. Dotted lines demarcate the perichondrium. Individual dots are from one bone. (Scale bar, 100 μm (*A* and *C*–*E*), 25 μm (*G*).) PHC, prehypertrophic chondrocytes; HC, hypertrophic chondrocytes; POC: primary ossification center. *P* values were calculated using a one-way ANOVA followed by Tukey's multiple comparisons test. *$P < 0.05$, **$P < 0.01$, NS, not significant. All data reflect mean ± SEM.

development and ECM processes (Fig. 5*E* and Dataset S2). Among the most affected were typical cartilage genes, such as *Col2a1*, *Col9a1, Col9a3, Col11a2*, *Chadl, Matn4*, *Trpv4* and *Hspg2,* signaling molecules *Tgfa, Nog* and transcription factors such as *Foxa3, Snai1* and *Sox8* (Dataset S1). To identify genes affected by haploinsufficiency or hypomorphic activity of SOX9^{Y440X}, we compared the DEGs in GFP$^+$ *Sox9*$^{+/CD}$ with those reported to be down-regulated in E11.5 and E12.5 *Sox9*$^{-/-}$ (homozygous null) limb buds (15). We found 29 down-regulated genes in common, among which were *Sox5,* SOX9 ECM gene targets such as *Col2a1*, *Col9a2, Col9a3, Col11a2*, *Matn4, Lect1,* and *Chadl,* and regulators of TGF/BMP signaling such as *Tgfa, Nog* (Dataset S3) (15, 20, 21, 48).

None of the up-regulated DEGs in *Sox9*$^{+/CD}$ GFP$^+$ cells overlapped with the *Sox9*$^{-/-}$ limb bud dataset (15) (Dataset S3). These *Sox9*$^{+/CD}$ GFP$^+$ DEGs included members of the WNT signaling pathway, such as the ligands *Wnt3, Wnt6, Wnt7a, Wnt9b*, as well as the pathway regulators, *Ctbrc1* and *Rnf43* that modulate Frizzled receptor activity to control WNT signaling (52) (53, 54) (Fig. 5*C*). These changes imply an overall increase in WNT signaling activity in the *Sox9*$^{+/CD}$ limb bud. Although in situ hybridization on E13.5 developing limbs showed increased expression of *Ihh, Ptch1, Mmp13, and Opn (Spp1)* (Fig. 2), these genes were not up-regulated in the transcriptome data. This discrepancy could be due to limitations of bulk RNA-seq to detect changes in gene expression occurring in a small fraction of the limb bud cells.

To identify direct SOX9 targets among the *Sox9*$^{+/CD}$ DEGs, we scanned +/− 10 kb of the promoter of every DEG for SOX9 binding peaks that had been identified in mouse rib chondrocytes and rat chondrosarcoma cells (20, 21). Of the DEGs, 163 down-regulated genes and 12 up-regulated genes were identified (Fig. 5*F*). Many of the down-regulated DEGs with SOX9-binding peaks encoded ECM proteins and enzymes involved in sulfation of proteoglycans, including *Col2a1*, *Col11a2*, *Chst11*, *Csgalnact1,* and *Papss2* (Dataset S4). Reduced expression of these genes should perturb ECM synthesis. Overall, many of the *Sox9*$^{+/Y440X}$ DEGs identified are associated with skeletal disorders (Datasets S5 and S6). For example, mutations in *SLC26A2,* an anion exchanger/anion channel and sulfate transporter, cause the chondrodysplasia, diastrophic dysplasia (24)

SOX9 acts in concert with partner factors, some of which are transcriptional regulators of chondrogenesis and osteogenesis and components of the HH, BMP, and WNT pathways (14). To investigate the impact of SOX9^{Y440X} on SOX9-partner regulation, we integrated bioinformatics analyses of the *Sox9*$^{+/Y440X}$ transcriptome with published SOX9 ChIP-seq chondrocyte/limb-bud datasets that had identified the binding motifs/peaks of SOX9 in conjunction with partners such as SOX5, SOX6, AP1, and GLI (20, 21, 23, 29, 55). We scanned 10 kb +/− of the promoter of every SOX9-bound *Sox9*$^{+/CD}$ GFP$^+$ DEG for AP1 binding peaks [BMP pathway, (23)] (*SI Appendix,* Fig. S7*D* and Dataset S4). Most SOX9-bound target DEGs were also SOX9-AP1 targets, e.g., *Col2a1, Nog* (down-regulated, 155) and *Wnt7b, Rspo1* (up-regulated, 8), suggesting SOX9^{Y440X} interferes with BMP/TGFβ signaling. GLI factors, the mediators of HH signaling, interact functionally with SOX9 in proliferating and PHCs (29). We scanned the *Sox9*$^{+/CD}$ GFP$^+$ DEGs for the previously described combination of SOX9 and GLI1 peaks (55) and found four, *Cxxc5, Csgalnact1, Wnk4* (down-regulated) and *Wnt7a* (up-regulated) (*SI Appendix,* Fig. S7*E* and Dataset S4). Interestingly, zinc-finger factor CXXC5 is a reported coordinator of BMP and WNT signaling (56). Since SOX9 regulates WNT signaling via moderating the availability of β-catenin, we also looked for GFP$^+$ DEGs with SOX9 binding peaks (20, 21) associated with the presence of SOX9/LEF/TCF consensus motifs (*SI Appendix,* Fig. S7*F* and Dataset S4). Four down-regulated DEGs, *Hr, Sh3tc2, Rgs3,* and *Slc26a2* were identified in the GFP$^+$ sample. Overall, these

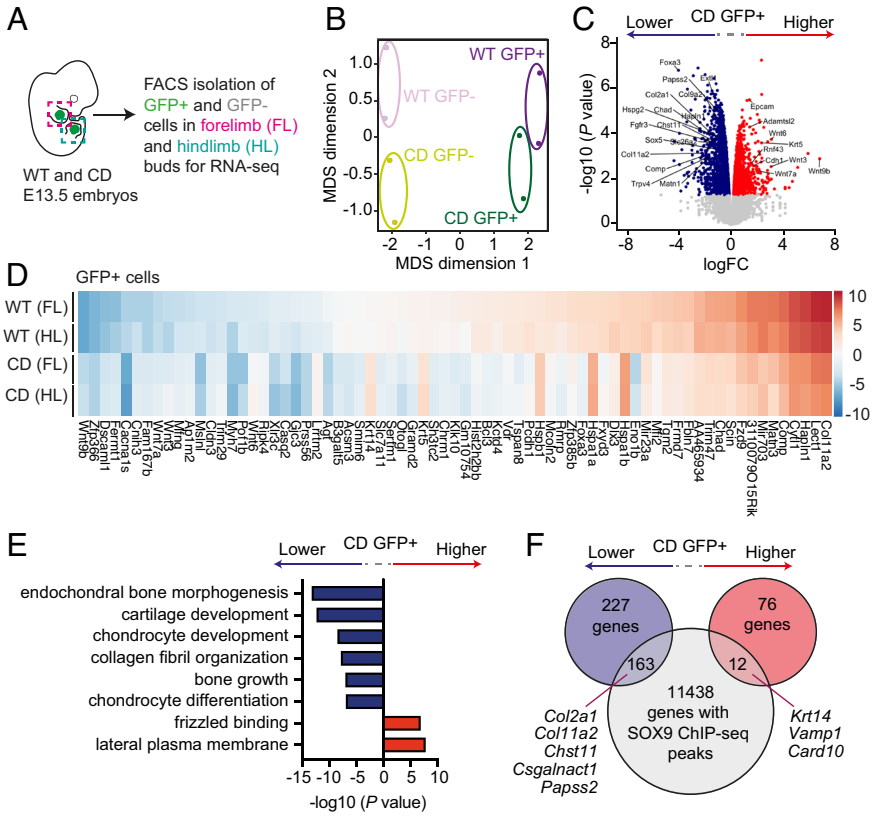

Fig. 5. RNA-seq reveals hypomorphic activity of SOX9^{Y440X}. (*A*) Forelimb (FL) and hindlimb (HL) were microdissected from E13.5 *Sox9*$^{+/IRES\text{-}GFP}$ (WT) and *Sox9*$^{+/CD}$ (CD) embryos and sorted to isolate *Sox9*-expressing population (GFP$^+$) and non-*Sox9*-expressing population (GFP$^-$) for RNA-seq. (*B*) Multidimensional scaling (MDS) plot of GFP$^+$ and GFP$^-$ populations from E13.5 WT and CD embryos. (*C*) Volcano plot showing genes that are differentially expressed between CD GFP$^+$ cells and WT GFP$^+$ cells. Blue and red dots represent genes that are down-regulated and up-regulated in CD GFP$^+$ cells, respectively. (*D*) Hierarchical clustering of top differentially expressed genes between samples, which have an absolute log fold change >1 and statistically significant differential expression at false discovery rate = 0.05. The scale bar shows the Z scores. (*E*) Gene Ontology analysis of enriched pathways in genes differentially expressed between CD GFP$^+$ cells and WT GFP$^+$ cells. Blue denotes pathways that are down-regulated, and red denotes pathways that are up-regulated in CD GFP$^+$ cells. (*F*) Venn diagram displaying the number of differentially expressed genes in CD GFP$^+$ cells that contain a SOX9 ChIP-seq peak within 10 kb of their promoter. Some specific gene names are shown as illustrative examples.

results implicate SOX9^{Y440X} as having impacts on multiple interacting pathways, notably BMP, HH, and WNT.

The ectopic ossification in the perichondrium of *Sox9*$^{+/CD}$ could be caused by noncell-autonomous signals from the chondrocytes. One way of assessing this possibility would be to assess whether there was an impact on GFP$^-$ cells in the *Sox9*$^{+/CD}$ limbs. We compared GFP$^+$ and GFP$^-$ DEGs that were down-regulated or up-regulated in mutant cells for overlap. The fraction of unique (non-overlapping) mutant GFP$^-$ DEGs was large (89%). Furthermore, the expression level of *Sox9* transcripts detected in GFP$^-$ cells was very low (only 5 to 8% of the levels in the GFP$^+$ fraction, *SI Appendix*, Fig. S6*B* and Dataset S1) consistent with the FACS enrichment of GFP$^+$ cells (*SI Appendix*, Fig. S7*C*).

Compared with WT, 425 genes were down-regulated in *Sox9*^{CD} GFP$^-$ cells, of which 48 (11%) were also among the 227 DEGs identified for *Sox9*^{CD}GFP$^+$ cells (*SI Appendix*, Fig. S7*G* and Dataset S7). GO term analyses of the *Sox9*^{CD}GFP$^-$ down-regulated DEGs showed enrichment for regulation of bone synthesis/remodeling including *Spp1* (osteopontin) (57) and *Inpp5d* (encoding for SH2-containing inositol-5′-phosphatase-1 (SHIP-1)) (*SI Appendix*, Fig. S7*H*). Interestingly, SHIP-1 is expressed in osteochondroprogenitors. SHIP-1 mutant mice show accelerated chondrocyte hypertrophy and premature formation of the secondary ossification center (58). Of the 85 DEGs up-regulated in GFP$^-$ mutant cells, 19 overlapped with the GFP$^+$ DEGs (76 genes) and included genes in the WNT pathway such as *Wnt3, Wnt6, Wnt7a, Wnt9b,* and *Gjb2* (Datasets S2 and S7). GO term analysis of up-regulated DEGs in *Sox9*^{CD} GFP$^-$ cells highlighted "cytokine–cytokine receptor interaction", which includes chemokine molecules (cytokines and their receptors e.g., *Ccl12, Cxcl2,* and *Cxcr5),* BMP pathway genes (e.g., *Gdf5, Bmpr1b, Bmpr2*) as well as genes classified under "frizzled binding" term, which included *Wnt3, Wnt6, Wnt7a, Wnt7b,* and *Wnt9b* (Dataset S2). These data suggest that many of genes differentially expressed in *Sox9*^{CD}GFP$^-$ cells could reflect noncell autonomous effects on promoting osteogenesis, especially the WNT pathway.

SOX9^{Y440X} Cannot Antagonize β-catenin-Mediated Transactivation of *Ihh*

The WNT/β-catenin pathway has been reported to positively regulate *Ihh* transcription in chondrocytes to control osteoblast development in the perichondrium (59–61). SOX9 antagonizes WNT signaling by interaction with β-catenin and promoting its degradation (62, 63). Therefore, we investigated whether SOX9^{Y440X} disrupts the normal interaction between SOX9 and β-catenin in antagonizing β-catenin-mediated transactivation of *Ihh*.

We found that ectopic expression of *Sox9* in HEK293 cells reduced β-catenin levels, whereas expression of *Sox9*^{Y440X} was unable to promote β-catenin degradation. Furthermore, coexpression of SOX9^{Y440X} resulted in reduced ability of SOX9 to induce β-catenin degradation (Fig. 6 *A* and *B*). In line with these in vitro results, immunostaining revealed increased numbers of HCs stained for unphosphorylated, active β-catenin in *C10Sox9*$^{CD/CD}$;*TdT* mutants compared with controls (Fig. 6 *C* and *D*). SOX9 has been reported to interact with β-catenin via its C-terminal transactivation domain (62). Consistent with the truncation of SOX9 in its transactivation domain, SOX9^{Y440X} did not coimmunoprecipitate with β-catenin. Most importantly, SOX9^{Y440X} interfered with the ability of SOX9 to interact with β-catenin, rendering it ineffective in promoting degradation of β-catenin

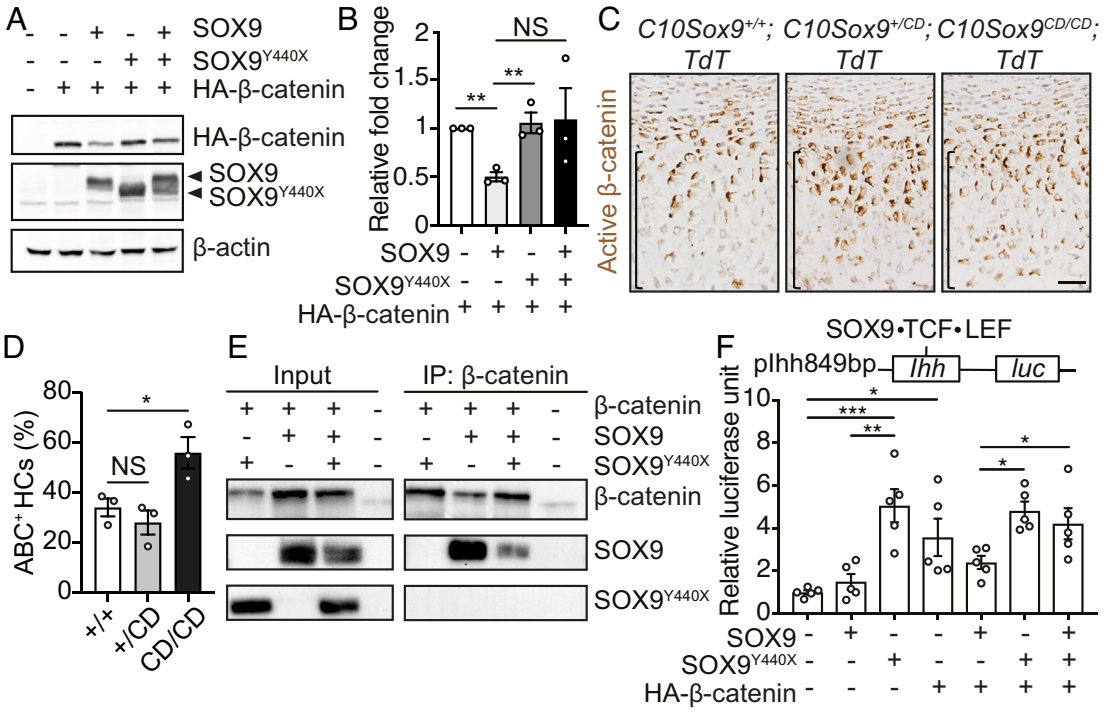

Fig. 6. SOX9^{Y440X} has impaired ability to degrade and antagonize β-catenin transactivity on *Ihh*. (*A*) Immunoblots of HA tagged β-catenin, SOX9, SOX9^{Y440X}, and β-actin on HEK293 cell extracts following transient transfection of the indicated expression plasmids (n = 3). (*B*) Quantification of HA-β-catenin in (*A*). (*C*) Immunohistochemistry for nonphosphorylated, active β-catenin (ABC) on E16.5 proximal tibia of mice of indicated genotype. Brackets denote hypertrophic zone. (*D*) Quantification of (*C*). Individual dots are from one bone. (*E*) 293T cells were transiently transfected with the indicated expression plasmids. Protein extracts were immunoprecipitated with anti-β-catenin antibody and probed with antibodies against SOX9 or SOX9^{Y440X} (n = 3). Input is shown. (*F*) Luciferase assay on 293T cells transiently transfected with the *Ihh* promoter luciferase reporter construct (pIhh849bp) in combination with the indicated expression plasmids. Individual dots are from one sample. *P* values were calculated using unpaired two-tailed Student's *t* test (*B* and *D*) and a one-way ANOVA followed by Tukey's multiple comparisons test (*F*). **P* < 0.05, ***P* < 0.01, ****P* < 0.005, NS, not significant. All data reflect mean ± SEM.

(Fig. 6*E*) and thereby would be predicted to result in an upregulation of β-catenin-TCF–LEF-mediated WNT signaling.

The *Ihh* promoter region contains TCF·LEF·SOX9-binding motifs (64). To assess whether the inability of SOX9^{Y440X} to target β-catenin for degradation leads to increased *Ihh* transactivation, we generated a luciferase reporter driven by an 849-bp fragment of mouse *Ihh* promoter region (pIhh-849-Luc) and measured reporter activity in transient transfection assays in HEK293 cells. While expression of SOX9 alone failed to transactivate luciferase, transfection-mediated expression of β-catenin and SOX9^{Y440X} individually and in combination, stimulated transactivation of the luciferase reporter (Fig. 6*F*). Furthermore, introduction of SOX9^{Y440X} led to an increased luciferase activity in SOX9 and β-catenin coexpressing cells (Fig. 6*F*). Cotransfection experiments showed that SOX9 inhibited β-catenin-mediated transactivation of the reporter, whereas SOX9^{Y440X} did not. Furthermore, introduction of SOX9^{Y440X} abrogated the repressive effect of SOX9 on β-catenin-mediated transactivation of the *Ihh* promoter (Fig. 6*F*). These data suggest that the presence of SOX9^{Y440X} interferes with the repressive activity of SOX9 on *Ihh*. In addition, SOX9^{Y440X} has reduced ability to mediate degradation of β-catenin, thereby enabling β-catenin to stimulate chondrocytic IHH signaling. Both of these scenarios contribute to campomelia.

SOX9^{Y440X} Exerts Hypomorphic and Dominant-Negative Interference Effects In Vivo

SOX9 transactivates genes as a DNA-dependent dimer (20, 30, 65–67). SOX9^{Y440X} retains intact DNA-binding and N-terminal dimerization domains. To gain mechanistic insights into the dominant interfering activity of SOX9^{Y440X}, we first performed chromatin immunoprecipitation assays on E13.5 limb lysates and demonstrated that SOX9^{Y440X} could bind to known SOX9 target genes such as *Acan*, *Col2a1,* and *Col10a1* with comparable efficiency to its wild-type counterpart (Fig. 7*A*). Coimmunoprecipitation assays on embryo extracts using WT SOX9 and SOX9^{Y440X} antibodies showed that the immunoprecipitated complexes contained both SOX9^{Y440X} and SOX9, suggesting mutant and WT SOX9 can dimerize in vivo (Fig. 7*B*). Since both SOX9 and SOX9^{Y440X} can bind DNA, altered regulation of SOX9 targets in the mutant could be due to loss of function (i.e., haploinsufficiency) or residual transactivation capacity (i.e., hypomorphism) of SOX9^{Y440X}. It is also possible that SOX9^{Y440X} binding to target regions negatively affects transactivation by WT SOX9, especially where homodimers are involved, resulting in a dominant-negative effect. We therefore assayed the transactivation ability of SOX9^{Y440X} in vivo using an established chicken neural tube electroporation technique that allows the introduction of exogenous proteins at defined dosage and combination (Fig. 7*C*). As expected, WT SOX9 stimulated the *Col2a1*-luciferase reporter in a dose-dependent manner (Fig. 7*D*), whereas SOX9^{Y440X} exhibited residual transactivity and increasing amounts did not enhance reporter activity (Fig. 7*E*). Notably, the addition of SOX9^{Y440X} significantly suppressed the induction of *Col2a1*-luciferase reporter by SOX9, indicative of a dominant-negative/interference action of SOX9^{Y440X} (Fig. 7*F*). In support of these findings, in situ hybridization revealed a marked reduction of *Col2a1* transcripts in many tissues of Sox9$^{+/CD}$ where *Col2a1* and *Sox9* are co-expressed (11), but the degree of downregulation in the developing neural folds, somites and otic vesicle, was more severe in *Sox9*$^{+/CD}$ embryos than in *Sox9*$^{+/-}$ (Fig. 7*G*).

To test the relevance of dominant-negative interference by SOX9^{Y440X} in vivo, we examined the transactivation ability of SOX9 or SOX9^{Y440X} in vivo using double transgenic mice. We utilized a *Hoxa1* enhancer element (*HoxaIII*) (68) that drives the expression

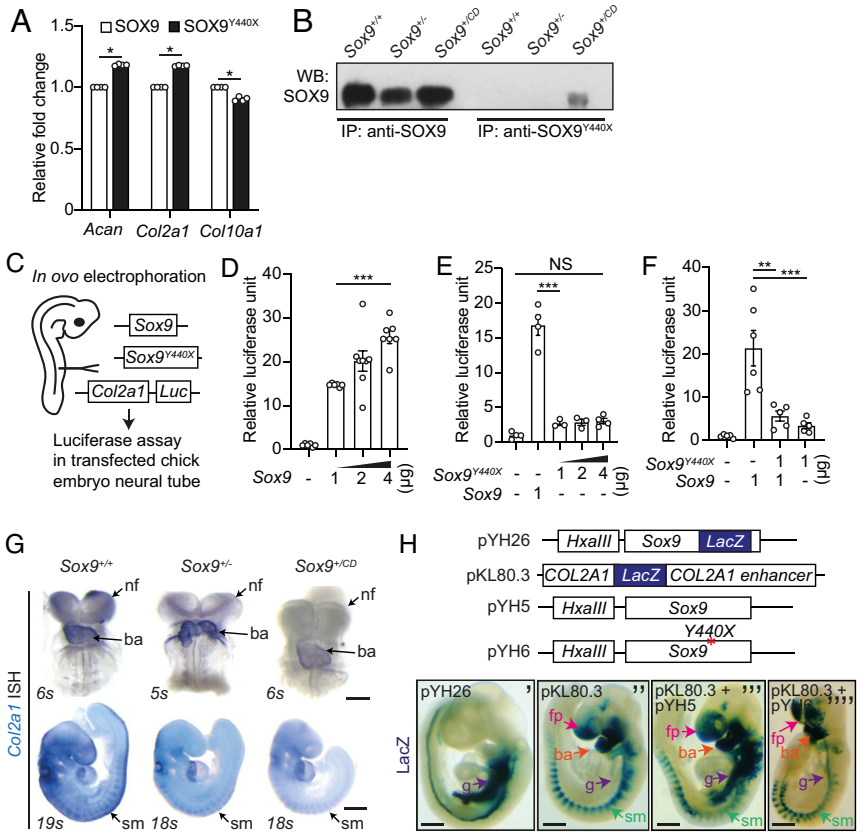

Fig. 7. Multifaceted molecular action of SOX9^{Y440X}. (*A*) Chromatin immunoprecipitation using antibodies against SOX9 and SOX9^{Y440X} to detect protein binding to *Acan*, *Col2a1* and *Col10a1* promoter regions. Individual dots are from one sample. (*B*) Immunoblots for SOX9 following immunoprecipitation with anti-SOX9 and anti-SOX9^{Y440X} antibodies on protein extracts of whole embryos of indicated genotypes (n = 3). (*C* to *F*) A *Col2a1-luc* reporter construct and the indicated expression plasmids were introduced to chicken neural tube through electroporation. The relative luciferase activity was compared with pCAGGS control in the absence of SOX9 and SOX9^{Y440X}. Individual dots are from one sample. (*G*) Whole mount in situ hybridization for *Col2a1* RNA in embryos of indicated genotypes and developmental stages. Somite number of embryos is provided (n = 3). (*H*) Schematic of expression plasmids and whole-mount X-gal staining of transgenic mouse embryos carrying the indicated expression plasmids (n = 3). nf, neural plate; ba, branchial arches; g, gut; fp, frontonasal process; sm, somites. (Scale bar, 100 µm (top row in *G*), 500 µm (bottom row in *G* and H).) *P* values were calculated using unpaired two-tailed Student's *t* test (*A*) and a one-way ANOVA followed by Tukey's multiple comparisons test (*D* to *F*). **P* < 0.05, ***P* < 0.01, ****P* < 0.005, NS, not significant. All data reflect mean ± SEM.

of a *LacZ* reporter (pYH26) to the notochord, floor plate, and gut epithelium with lower expression in the paraxial mesenchyme (Fig. 7*H′*) and transgenic mice carrying a *COL2A1* enhancer-*LacZ* reporter (pKL80.3)(17, 69) that expresses LacZ at characteristic *Col2a1*-expressing sites such as the notochord, paraxial mesenchyme, branchial arches, frontonasal process, and somites but not the gut (Fig. 7*H″*). The *HoxaIII* enhancer was linked to either *Sox9* (pYH5) or *Sox9*^{Y440X} (pYH6) and used to generate double transgenic mice in the background of the *Col2a1-LacZ* reporter gene. pYH5;pKL80.3 (*HoxaIII Sox9;Col2a1-LacZ)* double transgenic mice developed normally and the LacZ reporter was transactivated, where SOX9 was ectopically expressed in the periocular mesenchyme and gut (n = 3), consistent with previous demonstration of the direct transactivation of *COL2A1* (17). However in pYH6;pKL80.3 (*HoxaIII Sox9*^{Y440X};*Col2a1-LacZ*) double transgenic mice, reporter transactivation in the gut was not found (Fig. 7 *H‴* and *H⁗*). Importantly, *HoxaIII Sox9*^{Y440X};*Col2a1-LacZ* embryos displayed abnormalities such as the open neural tube, stunted branchial arches, and shortened frontonasal process, and the expression of *Col2a1-LacZ* in the notochord was diminished (Fig. 7*H⁗*, n = 17). Given that the double transgenic mouse embryos carried two alleles of endogenous WT *Sox9* and multiple copies of the *Sox9* (pYH5) or *Sox9*^{Y440X} (pYH6), a plausible explanation for the reduced reporter activity in the notochord and paraxial mesoderm in *HoxaIII Sox9*^{Y440X}; *Col2a1-LacZ* embryos and abnormal phenotypes was that exogenous SOX9^{Y440X} dominantly interfered with the endogenous SOX9 by competitive binding to the *Col2a1* enhancer within the *LacZ* transgene. Dominant interference of *HoxaIII*-driven *Sox9*^{Y440X} with endogenous *Sox9* activity in the neural tube, neural crest, and paraxial mesenchyme could cause the open neural tube and frontonasal and branchial arch abnormalities in the *Sox9*^{Y440X};*Col2a1-LacZ* embryos.

Discussion

When clear genotype–phenotype correlations are lacking in dominant syndromic disorders such as CD, the challenge lies in defining the underlying cellular and molecular mechanisms. Although the phenotypic impact of complete loss (homozygosity for a null mutation) of SOX9 function in different tissues is well known in the mouse, including the set of gene targets that are affected in the absence of the protein (7, 8, 14, 15, 26, 70–73), it is not clear what happens in heterozygotes, where the phenotypes are often dominant (14). The latter could be due to hypomorphic, dominant-negative, or neomorphic effects or a combination of more than one of these. In this study, we provide insights into the molecular mechanisms underlying the effects of heterozygosity for a SOX9 CD mutation with a truncated transactivation domain, on chondrocyte differentiation and osteogenesis. We tested the hypothesis that mechanisms other than haploinsufficiency operated in heterozygous mutations that are not null mutations. By comparing conditional mouse models of CD caused by a null mutation with the *Sox9*^{Y440X} mutation and a combination of transcriptome analyses, transactivation assays in cells and double transgenic mice, we provide evidence for a combination of dosage (haploinsufficiency/hypomorphism) and dominant-negative/neomorphic mechanisms that cause both cell

autonomous and noncell autonomous effects resulting in dysregulated osteogenesis and campomelia (Fig. 8*A*).

The skeletal hallmarks of CD and premature mineralization of bone in heterozygous *Sox9*$^{+/-}$ mice have been attributed to haploinsufficiency (39). Respiratory distress is the major cause of death in neonatal CD patients (74). Several aspects of the phenotype and molecular changes in *Sox9*$^{+/CD}$ mice are consistent with haploinsufficiency/hypomorphism. For example, the milder anomalies in tracheal cartilage and the survival of some *Sox9*$^{+/CD}$ mice are consistent with the residual transactivation activity for SOX9^{Y440X} shown in transactivation assays and double transgenic mice (38, 42).

Transcriptome profiling of *Sox9*$^{-/-}$ mutants and ChIP assays have identified thousands of SOX9 target genes in skeletal tissues (15, 26, 72). Our transcriptomic analyses in E13.5 *Sox9*$^{+/CD}$ limb buds revealed dysregulation of genes encoding ECM proteins and members of the BMP and WNT signaling pathways, implicating SOX9 as a master integrator of these pathways that regulate chondrocyte differentiation and osteogenesis (1, 6, 14). Comparison of gene expression in limb buds of E13.5 *Sox9*$^{+/CD}$ with that in E11.5 and E12.5 *Sox9*$^{-/-}$null mutants (15) identified down-regulated genes in common, especially DEGs encoding well-known SOX9 targets, such as ECM genes important for cartilage integrity (e.g., *Col2a1, Col9a3, Matn1,* and *Acan)*, transcription factors (e.g., *Sox5, Sox6, Foxc2,* and *Sema3d*) and a regulator of the BMP signaling pathways (*Nog)*. Many of the DEGs identified are associated with skeletal disorders, for example *ACAN, PAPSS2, CHST11,* and *SLC26A2* (24, 75–81) (Datasets S5 and S6). These down-regulated DEGs are consistent with haploinsufficiency, illustrating the dosage requirement for SOX9 and its importance for the synthesis of an appropriate ECM and for maintaining skeletal development.

Several lines of evidence suggest that mechanisms other than haploinsufficiency may apply for transactivation domain-truncating mutations like SOX9^{Y440X}. Transactivation assays in primary chondrocytes derived from CD patients have shown that, compared with null mutations, truncating *SOX9* mutations more severely reduced endogenous SOX9 transactivation. Aspects of the phenotypic severity and molecular changes in *Sox9*$^{+/CD}$ mice compared with *Sox9*$^{+/-}$ mice are consistent with alternative mechanisms.

First, skeletal development in *Sox9*$^{+/CD}$ mice was substantially more severely affected than in *Sox9*$^{+/-}$ mice. Molecular analysis in *Sox9*$^{+/CD}$ mutants revealed upregulation of HH signaling, enhanced expression of *Ihh* in the prehypertrophic and hypertrophic zones, and expanded and increased expression of the HH receptor gene *Ptch1* in PCs and perichondrium. The different expression domains of collagen X protein versus *Col10a1* transcripts in the hypertrophic zone, and premature OSX and *Col1a1/Opn/Mmp13* expression, all point to increased osteogenesis in the perichondrium/bone collar of mutant limbs, especially in the region of bowing. These changes were rarely observed in the *Sox9*$^{+/-}$ mice.

Second is the impact of *Sox9*^{Y440X} on SOX9-mediated degradation of ß-catenin in Sox9^{Y440X}-expressing cells. The SOX9 C terminus interacts with β-catenin to antagonize its activity via protein degradation, and in turn β-catenin positively regulates Ihh signaling in cartilage (59, 62–64). A functional link between HH signaling and WNT/ß-catenin signaling has been proposed (82) because HH signaling increases the expression of WNT ligands and enhance WNT/ß-catenin activation. Interestingly, activation of a β-catenin gain-of-function mutation in both immature chondrocytes and the perichondrium led to enhanced Ihh signaling and thickened perichondrial bone (59). Our transactivation assays showed SOX9^{Y440X} did not induce β-catenin degradation. The impaired β-catenin mediated suppression of transactivity on an *Ihh* promoter-driven reporter gene; the negative impact on transactivation of the *Col2a1* reporter in both chick embryos and double transgenic mouse embryos, are all consistent with a model of dominant-negative action of SOX9^{Y440X}.

Our study also provides insights into the cause of campomelia. Two mechanisms have been put forward to explain campomelia in CD: the presence of a hypoplastic cartilage primordium that forms a distorted template for bone, or malformation of the weakened cartilage and developing bone because of mechanical stresses from growing tendons and muscles (39, 83). The former could be due to deficiency in the cartilage matrix because of haploinsufficiency for SOX9. However, as the *C10Sox9*$^{CD/CD}$;*TdT* mice exhibited normal growth plate morphology and SOX9^{Y440X} is not expressed in tendon and muscle cells, additional mechanisms must underlie bone bowing. SOX9^{Y440X} caused asymmetric perichondrial hyperossification resulting in bowed limbs in both constitutive and conditional *Sox9*$^{+/CD}$ and *C10Sox9*$^{CD/CD}$;*TdT* mutants. The extent of perichondrial hyperossification correlated with the severity of campomelia, supporting a causative relationship between the two. We hypothesize that the aberrant perichondrial bone mass disturbs the growth axis of the long bone, causing curvature of the cartilage template and the ensuing endochondral bone. Furthermore, campomelia likely arises from the combined contribution of abnormal chondrocyte differentiation and perichondrial hyperossification acting in parallel.

An important question arising is whether the campomelia in *Sox9*$^{+/CD}$ is the result of cell-autonomous or noncell autonomous effects or a combination of both. The campomelia and enhanced osteogenesis in the E13.5 perichondrium of HC-specific *Sox9*$^{CD/CD}$ homozygotes, in which *Sox9*^{Y440X} is activated in HCs but not the perichondrium, raises the possibility that part of the impact of the mutant SOX9 is a noncell autonomous upregulation of *Ptch1*-mediated HH signaling and up-regulation of WNT pathway genes and chemokines such as CXCL12, which signal to non-*Sox9*^{Y440X} expressing cells in the perichondrium leading to the perichondrial bone mass.

Proteoglycans and their sulfation have been reported to be necessary for proper HH signaling in the developing growth plate (84), and are thought to modulate the range and gradient of HH signaling in the ECM. The impact of *Sox9*^{Y440X} on expression of many genes encoding ECM proteins, including collagens (*Col2a1*, *Col11a2*) and proteoglycans (*Hspg2*, *Comp*, *Chad*), and others that contribute to their biosynthesis, e.g., enzymes involved in sulfation of proteoglycans (*Slc26a2, Papss2,* and *Chst11),* would be predicted to result in an abnormal ECM, which could perturb growth factor/morphogen signaling.

The reasons for the deviation of the orientation *Sox9*$^{+/CD}$ growth plate and asymmetric synthesis of ectopic bone associated with the bowing are unknown. A question to address in future is the relevance of the upregulation of the frizzled pathway found in both GFP^{-} and GFP^{+} cells. Upregulation of *Wnt9b* could affect planar cell polarity (PCP) (85) in the *Sox9*$^{+/CD}$ mutant growth plate contributing to the campomelia. Noncell autonomous upregulation of WNT pathway genes in the perichondrium could cause hyperossification, contributing to the ectopic ossification. It is also possible that changes in apicobasal polarity contribute to the asymmetric perichondrial osteogenesis. *Col9a3* expression was down-regulated and notably *Sox9* deletion in the choroid plexus reduced *Col9a3* expression and disrupted apicobasal polarity (86). Whether the down-regulated expression of *Col9a3* and other ECM genes in *Sox9*$^{+/CD}$ limb buds similarly affect apicobasal polarity leading to aberrant osteogenesis warrants further investigation.

In summary, we propose a model (Fig. 8) in which, for some *SOX9* CD mutations, rather than global haploinsufficiency for SOX9, and in a manner that is dependent on the target gene and cell context, both haploinsufficiency/hypomorphism and dominant-negative mechanisms can apply. Furthermore, the final phenotype may arise from both cell autonomous and noncell autonomous effects. Such a molecular model provides insights into the role of SOX9 in skeletal morphogenesis, and the control of chondroosteogenesis that influences bone shape.

Since *Sox9* has many roles in development and in adult stem cells in diverse tissues, the principles we have uncovered demonstrate the importance of determining the appropriate cellular context of a single causal mutation in order to interpret the underlying mechanisms of syndromes in which there are multiple disease-related cellular phenotypes. The findings therefore extend beyond skeletal development, to the other organs where SOX9 has important roles, such as in sex

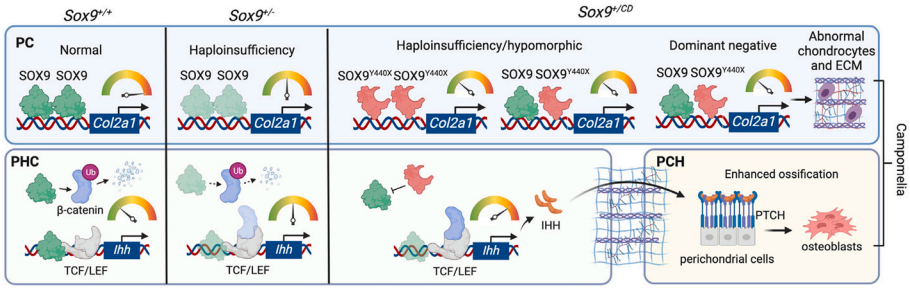

Fig. 8. A model of haploinsufficiency/hypomorphism and dominant-negative impact of SOX9^{Y440X} in perturbing endochondral bone development. (*A*) Haploinsufficiency for SOX9 in *Sox9*$^{+/-}$ mutants. SOX9^{Y440X} retains DNA binding, dimerization, and residual transactivation capacity (acting as a hypomorph). It can also compete with SOX9 in binding to SOX9 targets (e.g., *Col2a1* and other ECM genes) and act in a dominant-negative manner to further reduce the expression of key chondrocyte developmental genes. Furthermore, the C terminus truncated SOX9^{Y440X} has impaired ability to interact with and promote degradation of β-catenin resulting in enhanced activity of TCF/LEF on Wnt targets such as *Ihh*. IHH production is stimulated, acts noncell autonomously, leading to enhanced osteoblastic differentiation of perichondrial cells. Collectively, action of SOX9^{Y440X} disturbs the highly regulated process of chondrogenesis and ECM deposition, and enhances ossification in the perichondrium, which together promote the development of campomelia. Image created using BioRender.com.

determination, inner ear, kidney, and neural development. The findings are also relevant to understanding the molecular role of *SOX9* in acquired diseases (87), controls of chondroosteogenesis, which are reiterated in different clinical scenarios such as during normal fracture healing and in other diseases where repair is impaired and bone bending occurs such as in osteogenesis imperfecta. The mechanistic principles are also applicable to other developmentally important transcription factors that work with partners and have significance for tissue-specific effects in a broad spectrum of diseases.

Materials and Methods

Detailed description of standard methods is in *SI Appendix*.

***Sox9*$^{floxed\text{-}Y440X}$ Mice.** *Sox9*$^{floxed\text{-}Y440X}$ mice were generated from gene targeted ES cells (*SI Appendix*, Fig. S1*A*). The targeting vector contained mouse genomic *Sox9* sequences including exons 1, 2, and a loxP-flanked exon 3, followed by a mutated exon 3 (exon 3) carrying a nonsense mutation *Y440X* and *IRES2-EGFP* sequences, and a FRT-flanked pgk-neo cassette inserted before the 3′flanking sequences. Details are shown in *SI Appendix*, Fig. S1 *B–G*.

SOX9^{Y440X} Antibody. *Sox9*^{Y440X} mutation leads to the production of a truncated SOX9 protein of 439 amino acids compared with a wild type of 507 amino acids. The peptide sequence chosen for raising the antibody consists of 14 a.a. (426 to 439), YSPSYPPITRSQYD. Peptide synthesis and antibody production were by Covalab UK Ltd. (www.covalab.co.uk). See *SI Appendix* for details.

Mouse Phenotype Characterization, Transactivation, Luciferase, and ChIP Assays. Standard methods were used, see *SI Appendix*

RNA-seq. E13.5 mouse limb buds (4 to 6 pairs of forelimb (FL) and the hindlimb (HL) were harvested from *Sox9*$^{+/IRES\text{-}EGFP}$ (WT) and *Sox9*$^{+/Y440X\text{-}IRES\text{-}EGFP}$ (CD) and digested with 0.05% Collagenase Type II (Worthington Biochemical, Cat. CLS-2) and 0.05% Neutral protease (Worthington Biochemical, Cat. LSO2100) in DMEM for <1 h at 37 °C. For RNA-sequencing, 100 ng total RNA was used as input for each sample. cDNA libraries were prepared by TruSeq Stranded mRNA Sample Prep Kit (Illumina) according to the manufacturer's instructions. PairEnd sequencing of 101 bp was done using the HiSeq 1500 Sequencer Model. The Illumina HiSeq SBS Kit v4 and the HiSeq PE Cluster Kit v4 cBot were used for cluster generation on the flow cell. See *SI Appendix*or details of bioinformatics analyses.

Data, Materials, and Software Availability. [RNA sequencing] data have been deposited in [GEO database; Github] (GSE201261; https://github.com/fuxialexander/sox9). All study data are included in the article and/or *SI Appendix*.

ACKNOWLEDGMENTS. We thank Danny Chan, Kenneth Cheung, Peter Koopman, Chi Chung Hui, Michael Zhang, and Reinhard Faessler for advice and helpful discussion. We thank Tom Lufkin for the gift of the HoxaII enhancer vector. This work was supported by grants to K.S.E.C. from the Research Grants Council and University Grants Council of Hong Kong: HKU7247/98M, HKU7222/97M, AoE/M-04/04, T12-708/12N, and the Jimmy and Emily Tang Professorship. T.Y.T. was supported by an Australian NHMRC Neil Hamilton Fairley Overseas Exchange Fellowship 607431.

Author affiliations: [a]School of Biomedical Sciences, The University of Hong Kong, Li Ka Shing Faculty of Medicine, Hong Kong, China; [b]Department of Computer Science and Engineering, The Chinese University of Hong Kong, New Territories, Shatin, Hong Kong SAR, China; and [c]Francis Crick Institute, London NW1 1AT, UK

[1]T.Y.K.A. and R.K.H.Y. contributed equally to this work.

[2]Present address: Advanced Technology and Biology and Inflammation Division, Walter and Eliza Hall Institute of Medical Research, Parkville, VIC 3052, Australia.

[3]Present address: Victorian Clinical Genetics Services, Murdoch Children's Research Institute, University of Melbourne, Parkville, VIC 3052, Australia.

[4]Present address: Department of Biomedical Informatics, Columbia University, New York, NY 10032.

[5]Present address: Research & Development Centre, United Cell Biotechnology Co., Ltd, Shanghai 201206, People's Republic of China.

[6]Present address: Center for Systems Biology, The University of Texas at Dallas, Richardson, TX 75080.

[7]Present address: Sanford Burnham Prebys Medical Discovery Institute, La Jolla, CA 92037.

[8]To whom correspondence may be addressed. Email: kathycheah@hku.hk.

1. G. Karsenty, H. M. Kronenberg, C. Settembre, Genetic control of bone formation. *Annu. Rev. Cell Dev. Biol.* **25**, 629–648 (2009).
2. K. Y. Tsang, K. S. Cheah, The extended chondrocyte lineage: Implications for skeletal homeostasis and disorders. *Curr. Opin. Cell Biol.* **61**, 132–140 (2019).
3. L. Yang, K. Y. Tsang, H. C. Tang, D. Chan, K. S. Cheah, Hypertrophic chondrocytes can become osteoblasts and osteocytes in endochondral bone formation. *Proc. Natl. Acad. Sci. U.S.A.* **111**, 12097–12102 (2014).
4. X. Zhou *et al.*, Chondrocytes transdifferentiate into osteoblasts in endochondral bone during development, postnatal growth and fracture healing in mice. *PLoS Genet.* **10**, e1004820 (2014).
5. G. R. Mortier *et al.*, Nosology and classification of genetic skeletal disorders: 2019 revision. *Am. J. Med. Genet. A* **179**, 2393–2419 (2019).
6. R. K. H. Yip, D. Chan, K. S. E. Cheah, Mechanistic insights into skeletal development gained from genetic disorders. *Curr. Top. Dev. Biol.* **133**, 343–385 (2019).
7. H. Akiyama, M. C. Chaboissier, J. F. Martin, A. Schedl, B. de Crombrugghe, The transcription factor Sox9 has essential roles in successive steps of the chondrocyte differentiation pathway and is required for expression of Sox5 and Sox6. *Genes Dev.* **16**, 2813–2828 (2002).
8. W. Bi, J. M. Deng, Z. Zhang, R. R. Behringer, B. de Crombrugghe, Sox9 is required for cartilage formation. *Nat. Genet.* **22**, 85–89 (1999).
9. E. Wright *et al.*, The sry-related gene Sox9 is expressed during chondrogenesis in mouse embryos. *Nat. Genet.* **9**, 15–20 (1995).
10. Q. Zhao, H. Eberspaecher, V. Lefebvre, B. De Crombrugghe, Parallel expression of Sox9 and Col2a1 in cells undergoing chondrogenesis. *Dev. Dyn.* **209**, 377–386 (1997).
11. L. J. Ng *et al.*, SOX9 binds DNA, activates transcription, and coexpresses with type II collagen during chondrogenesis in the mouse. *Dev. Biol.* **183**, 108–121 (1997).
12. H. Akiyama *et al.*, Osteo-chondroprogenitor cells are derived from Sox9 expressing precursors. *Proc. Natl. Acad. Sci. U.S.A.* **102**, 14665–14670 (2005).

13. P. Dy *et al.*, Sox9 directs hypertrophic maturation and blocks osteoblast differentiation of growth plate chondrocytes. *Dev. Cell* **22**, 597–609 (2012).
14. V. Lefebvre, M. Angelozzi, A. Haseeb, SOX9 in cartilage development and disease. *Curr. Opin. Cell Biol.* **61**, 39–47 (2019).
15. C. F. Liu, M. Angelozzi, A. Haseeb, V. Lefebvre, SOX9 is dispensable for the initiation of epigenetic remodeling and the activation of marker genes at the onset of chondrogenesis. *Development* **145**, dev164459 (2018).
16. V. Lefebvre, Roles and regulation of SOX transcription factors in skeletogenesis. *Curr. Top. Dev. Biol.* **133**, 171–193 (2019).
17. D. M. Bell *et al.*, SOX9 directly regulates the type-II collagen gene. *Nat. Genet.* **16**, 174–178 (1997).
18. V. Lefebvre, W. Huang, V. R. Harley, P. N. Goodfellow, B. de Crombrugghe, SOX9 is a potent activator of the chondrocyte-specific enhancer of the pro alpha1(II) collagen gene. *Mol. Cell Biol.* **17**, 2336–2346 (1997).
19. Y. Han, V. Lefebvre, L-Sox5 and Sox6 drive expression of the aggrecan gene in cartilage by securing binding of Sox9 to a far-upstream enhancer. *Mol. Cell Biol.* **28**, 4999–5013 (2008).
20. S. Ohba, X. He, H. Hojo, A. P. McMahon, Distinct transcriptional programs underlie Sox9 regulation of the mammalian chondrocyte. *Cell Rep.* **12**, 229–243 (2015).
21. C. F. Liu, V. Lefebvre, The transcription factors SOX9 and SOX5/SOX6 cooperate genome-wide through super-enhancers to drive chondrogenesis. *Nucleic Acids Res.* **43**, 8183–8203 (2015).
22. L. C. Bridgewater, V. Lefebvre, B. de Crombrugghe, Chondrocyte-specific enhancer elements in the Col11a2 gene resemble the Col2a1 tissue-specific enhancer. *J. Biol. Chem.* **273**, 14998–15006 (1998).
23. X. He, S. Ohba, H. Hojo, A. P. McMahon, AP-1 family members act with Sox9 to promote chondrocyte hypertrophy. *Development* **143**, 3012–3023 (2016).
24. S. L. Alper, A. K. Sharma, The SLC26 gene family of anion transporters and channels. *Mol. Aspects Med.* **34**, 494–515 (2013).
25. G. Zhou *et al.*, Dominance of SOX9 function over RUNX2 during skeletogenesis. *Proc. Natl. Acad. Sci. U.S.A.* **103**, 19004–19009 (2006).
26. A. Haseeb *et al.*, SOX9 keeps growth plates and articular cartilage healthy by inhibiting chondrocyte dedifferentiation/osteoblastic redifferentiation. *Proc. Natl. Acad. Sci. U.S.A.* **118**, e2019152118 (2021).
27. V. Y. Leung *et al.*, SOX9 governs differentiation stage-specific gene expression in growth plate chondrocytes via direct concomitant transactivation and repression. *PLoS Genet.* **7**, e1002356 (2011).
28. A. Cheng, P. G. Genever, SOX9 determines RUNX2 transactivity by directing intracellular degradation. *J. Bone. Miner. Res.* **25**, 2680–2689 (2010).
29. Z. Tan *et al.*, Synergistic co-regulation and competition by a SOX9-GLI-FOXA phasic transcriptional network coordinate chondrocyte differentiation transitions. *PLoS Genet.* **14**, e1007346 (2018).
30. P. Bernard *et al.*, Dimerization of SOX9 is required for chondrogenesis, but not for sex determination. *Hum. Mol. Genet.* **12**, 1755–1765 (2003).
31. M. Lewandoski, E. N. Meyers, G. R. Martin, Analysis of Fgf8 gene function in vertebrate development. *Cold Spring Harb. Symp. Quant. Biol.* **62**, 159–168 (1997).
32. E. Sock *et al.*, Loss of DNA-dependent dimerization of the transcription factor SOX9 as a cause for campomelic dysplasia. *Hum. Mol. Genet.* **12**, 1439–1447 (2003).
33. M. Leipoldt *et al.*, Two novel translocation breakpoints upstream of SOX9 define borders of the proximal and distal breakpoint cluster region in campomelic dysplasia. *Clin. Genet.* **71**, 67–75 (2007).
34. G. V. Velagaleti *et al.*, Position effects due to chromosome breakpoints that map approximately 900 Kb upstream and approximately 1.3 Mb downstream of SOX9 in two patients with campomelic dysplasia. *Am. J. Hum. Genet.* **76**, 652–662 (2005).
35. D. Pfeifer *et al.*, Campomelic dysplasia translocation breakpoints are scattered over 1 Mb proximal to SOX9: Evidence for an extended control region. *Am. J. Hum. Genet.* **65**, 111–124 (1999).
36. C. Kwok *et al.*, Mutations in SOX9, the gene responsible for Campomelic dysplasia and autosomal sex reversal. *Am. J. Hum. Genet.* **57**, 1028–1036 (1995).
37. S. Unger, G. Scherer, A. Superti-Furga, "Campomelic dysplasia" in *GeneReviews((R))*, M. P. Adam, Eds. (University of Washington, Seattle (WA), 1993).
38. J. Meyer *et al.*, Mutational analysis of the SOX9 gene in campomelic dysplasia and autosomal sex reversal: Lack of genotype/phenotype correlations. *Hum. Mol. Genet.* **6**, 91–98 (1997).
39. W. Bi *et al.*, Haploinsufficiency of Sox9 results in defective cartilage primordia and premature skeletal mineralization. *Proc. Natl. Acad. Sci. U.S.A.* **98**, 6698–6703 (2001).
40. A. E. von Bohlen *et al.*, A mutation creating an upstream initiation codon in the SOX9 5′ UTR causes acampomelic campomelic dysplasia. *Mol. Genet. Genomic. Med.* **5**, 261–268 (2017).
41. R. M. Hageman, F. J. Cameron, A. H. Sinclair, Mutation analysis of the SOX9 gene in a patient with campomelic dysplasia. *Hum. Mutat.* (suppl. 1) **11**, S112–S113 (1998).
42. R. Pop, M. V. Zaragoza, M. Gaudette, U. Dohrmann, G. Scherer, A homozygous nonsense mutation in SOX9 in the dominant disorder campomelic dysplasia: A case of mitotic gene conversion. *Hum. Genet.* **117**, 43–53 (2005).
43. T. Wagner *et al.*, Autosomal sex reversal and campomelic dysplasia are caused by mutations in and around the SRY-related gene SOX9. *Cell* **79**, 1111–1120 (1994).
44. F. Csukasi *et al.*, Dominant-negative SOX9 mutations in campomelic dysplasia. *Hum. Mutat.* **40**, 2344–2352 (2019).
45. K. Y. Tsang *et al.*, Surviving endoplasmic reticulum stress is coupled to altered chondrocyte differentiation and function. *PLoS Biol.* **5**, e44 (2007).
46. C. Maes *et al.*, Osteoblast precursors, but not mature osteoblasts, move into developing and fractured bones along with invading blood vessels. *Dev. Cell* **19**, 329–344 (2010).
47. L. Madisen *et al.*, A robust and high-throughput Cre reporting and characterization system for the whole mouse brain. *Nat. Neurosci.* **13**, 133–140 (2010).
48. H. Hojo *et al.*, Hedgehog-Gli activators direct osteo-chondrogenic function of bone morphogenetic protein toward osteogenesis in the perichondrium. *J. Biol. Chem.* **288**, 9924–9932 (2013).
49. B. St-Jacques, M. Hammerschmidt, A. P. McMahon, Indian hedgehog signaling regulates proliferation and differentiation of chondrocytes and is essential for bone formation. *Genes Dev.* **13**, 2072–2086 (1999).
50. F. Long *et al.*, Ihh signaling is directly required for the osteoblast lineage in the endochondral skeleton. *Development* **131**, 1309–1318 (2004).
51. L. Nel-Themaat *et al.*, Morphometric analysis of testis cord formation in Sox9-EGFP mice. *Dev. Dyn.* **238**, 1100–1110 (2009).
52. S. Yamamoto *et al.*, Cthrc1 selectively activates the planar cell polarity pathway of Wnt signaling by stabilizing the Wnt-receptor complex. *Dev. Cell* **15**, 23–36 (2008).
53. B. K. Koo *et al.*, Tumour suppressor RNF43 is a stem-cell E3 ligase that induces endocytosis of Wnt receptors. *Nature* **488**, 665–669 (2012).
54. G. Colozza, B. K. Koo, Ub and Dub of RNF43/ZNRF3 in the WNT signalling pathway. *EMBO Rep.* **22**, e52970 (2021).
55. S. A. Vokes, H. Ji, W. H. Wong, A. P. McMahon, A genome-scale analysis of the cis-regulatory circuitry underlying sonic hedgehog-mediated patterning of the mammalian limb. *Genes Dev.* **22**, 2651–2663 (2008).
56. X. Xiong, S. Tu, J. Wang, S. Luo, X. Yan, CXXC5: A novel regulator and coordinator of TGF-beta, BMP and Wnt signaling. *J. Cell Mol. Med.* **23**, 740–749 (2019).
57. Y. Asou *et al.*, Osteopontin facilitates angiogenesis, accumulation of osteoclasts, and resorption in ectopic bone. *Endocrinology* **142**, 1325–1332 (2001).
58. E. Y. So *et al.*, Lipid phosphatase SHIP-1 regulates chondrocyte hypertrophy and skeletal development. *J. Cell Physiol.* **235**, 1425–1437 (2020).
59. D. Y. Dao *et al.*, Cartilage-specific beta-catenin signaling regulates chondrocyte maturation, generation of ossification centers, and perichondrial bone formation during skeletal development. *J. Bone Miner. Res.* **27**, 1680–1694 (2012).
60. K. K. Mak, M. H. Chen, T. F. Day, P. T. Chuang, Y. Yang, Wnt/beta-catenin signaling interacts differentially with Ihh signaling in controlling endochondral bone and synovial joint formation. *Development* **133**, 3695–3707 (2006).
61. S. J. Rodda, A. P. McMahon, Distinct roles for Hedgehog and canonical Wnt signaling in specification, differentiation and maintenance of osteoblast progenitors. *Development* **133**, 3231–3244 (2006).
62. H. Akiyama *et al.*, Interactions between Sox9 and beta-catenin control chondrocyte differentiation. *Genes Dev.* **18**, 1072–1087 (2004).
63. L. Topol, W. Chen, H. Song, T. F. Day, Y. Yang, Sox9 inhibits Wnt signaling by promoting beta-catenin phosphorylation in the nucleus. *J. Biol. Chem.* **284**, 3323–3333 (2009).
64. B. L. Huang, S. M. Brugger, K. M. Lyons, Stage-specific control of connective tissue growth factor (CTGF/CCN2) expression in chondrocytes by Sox9 and beta-catenin. *J. Biol. Chem.* **285**, 27702–27712 (2010).
65. L. C. Bridgewater *et al.*, Adjacent DNA sequences modulate Sox9 transcriptional activation at paired Sox sites in three chondrocyte-specific enhancer elements. *Nucleic Acids Res.* **31**, 1541–1553 (2003).
66. M. A. Genzer, L. C. Bridgewater, A Col9a1 enhancer element activated by two interdependent SOX9 dimers. *Nucleic Acids Res.* **35**, 1178–1186 (2007).
67. F. Coustry *et al.*, The dimerization domain of SOX9 is required for transcription activation of a chondrocyte-specific chromatin DNA template. *Nucleic Acids Res.* **38**, 6018–6028 (2010).
68. M. Frasch, X. Chen, T. Lufkin, Evolutionary-conserved enhancers direct region-specific expression of the murine Hoxa-1 and Hoxa-2 loci in both mice and Drosophila. *Development* **121**, 957–974 (1995).
69. K. K. Leung, L. J. Ng, K. K. Ho, P. P. Tam, K. S. Cheah, Different cis-regulatory DNA elements mediate developmental stage- and tissue-specific expression of the human COL2A1 gene in transgenic mice. *J. Cell Biol.* **141**, 1291–1300 (1998).
70. V. C. Garside *et al.*, SOX9 modulates the expression of key transcription factors required for heart valve development. *Development* **142**, 4340–4350 (2015).
71. N. Gonen, R. Lovell-Badge, The regulation of Sox9 expression in the gonad. *Curr. Top Dev. Biol.* **134**, 223–252 (2019).
72. M. Tsingas *et al.*, Sox9 deletion causes severe intervertebral disc degeneration characterized by apoptosis, matrix remodeling, and compartment-specific transcriptomic changes. *Matrix Biol.* **94**, 110–133 (2020).
73. F. Barrionuevo, M. M. Taketo, G. Scherer, A. Kispert, Sox9 is required for notochord maintenance in mice. *Dev. Biol.* **295**, 128–140 (2006).
74. S. Mansour *et al.*, The phenotype of survivors of campomelic dysplasia. *J. Med. Genet.* **39**, 597–602 (2002).
75. B. G. Gibson, M. D. Briggs, The aggrecanopathies; An evolving phenotypic spectrum of human genetic skeletal diseases. *Orphanet J. Rare Dis.* **11**, 86 (2016).
76. N. Miyake *et al.*, PAPSS2 mutations cause autosomal recessive brachyolmia. *J. Med. Genet.* **49**, 533–538 (2012).
77. M. Kluppel, T. N. Wight, C. Chan, A. Hinek, J. L. Wrana, Maintenance of chondroitin sulfation balance by chondroitin-4-sulfotransferase 1 is required for chondrocyte development and growth factor signaling during cartilage morphogenesis. *Development* **132**, 3989–4003 (2005).
78. R. M. K. Shabbir, G. Nalbant, N. Ahmad, S. Malik, A. Tolun, Homozygous CHST11 mutation in chondrodysplasia, brachydactyly, overriding digits, clino-symphalangism and synpolydactyly. *J. Med. Genet.* **55**, 489–496 (2018).
79. J. Hastbacka *et al.*, The diastrophic dysplasia gene encodes a novel sulfate transporter: Positional cloning by fine-structure linkage disequilibrium mapping. *Cell* **78**, 1073–1087 (1994).
80. M. Park *et al.*, Multiple roles of the SO4(2-)/Cl-/OH- exchanger protein Slc26a2 in chondrocyte functions. *J. Biol. Chem.* **289**, 1993–2001 (2014).
81. A. Superti-Furga *et al.*, Achondrogenesis type IB is caused by mutations in the diastrophic dysplasia sulphate transporter gene. *Nat. Genet.* **12**, 100–102 (1996).
82. Q. Deng *et al.*, Activation of hedgehog signaling in mesenchymal stem cells induces cartilage and bone tumor formation via Wnt/beta-Catenin. *Elife* **8**, e50208 (2019).
83. A. Sharir, T. Stern, C. Rot, R. Shahar, E. Zelzer, Muscle force regulates bone shaping for optimal load-bearing capacity during embryogenesis. *Development* **138**, 3247–3259 (2011).
84. M. Cortes, A. T. Baria, N. B. Schwartz, Sulfation of chondroitin sulfate proteoglycans is necessary for proper Indian hedgehog signaling in the developing growth plate. *Development* **136**, 1697–1706 (2009).
85. C. M. Karner *et al.*, Wnt9b signaling regulates planar cell polarity and kidney tubule morphogenesis. *Nat. Genet.* **41**, 793–799 (2009).
86. K. I. Vong *et al.*, SOX9-COL9A3-dependent regulation of choroid plexus epithelial polarity governs blood-cerebrospinal fluid barrier integrity. *Proc. Natl. Acad. Sci. U.S.A.* **118**, e2009568118 (2021).
87. J. Pritchett, V. Athwal, N. Roberts, N. A. Hanley, K. P. Hanley, Understanding the role of SOX9 in acquired diseases: Lessons from development. *Trends Mol. Med.* **17**, 166–174 (2011).